Università degli Studi di Padova

Dipartimento di Ingegneria Industriale

Corso di Laurea Magistrale in Ingeneria Aerospaziale

Optimization of Helicon Plasma thruster with a Global Model

Relatore
Prof. Daniele Pavarin

Correlatore
Dott. Ing. Mirko Magarotto

Candidato
Alessandro Berlanda
matr. 2023814

Anno Accademico 2022–2023

Università degli Studi di Padova

Dipartimento di Ingegneria Industriale

Corso di Laurea Magistrale in Ingeneria Aerospaziale

Optimization of Helicon Plasma thruster with a Global Model

Relatore
Prof. Daniele Pavarin

Correlatore
Dott. Ing. Mirko Magarotto

Candidato
Alessandro Berlanda
matr. 2023814

Anno Accademico 2022–2023

Abstract

Electric propulsion represents the new technological frontier of space propulsion; although it is a technology still under development and with major performance limitations, in some specific cases it presents aspects that are absolutely advantageous. The possibility of generating thrust using electricity is one of these: in Earth orbit solar radiation is such as to provide a constant supply of energy that would not be possible to exploit with chemical engines. On the other hand, the chemical engine still represents the most effective method for a launcher to carry loads into orbit, since the thrust of an electric motor has not yet reached levels capable of fulfilling this task. Electric thrusters are mainly divided into two classes, cathode thrusters and cathodeless thrusters. The thruster that will be studied in this thesis belongs to the category of cathodeless thrusters, and more specifically we talk about Helicon Plasma Thrusters. The name of these thrusters derives from the helical shape that the charged particles draw with their trajectory when immersed in a magnetic field. The purpose of this thesis will be to optimize a 50W Helicon Plasma Thruster using the so-called "Global Model", a code written in Matlab language which describes the physics of the plasma and subsequently determines the propulsive performance of the engine itself. The Global Model allows to solve two differential equations of the second order which are respectively the mass balance equation and the energy equation. It is from the solution of these equations that it subsequently becomes possible, through another block of code called "Propulsion Model", to determine the propulsive characteristics of the engine.

Our analysis focuses first on the choice of the most suitable propellant for our purposes. The most used gases for electric propulsion are Argon, Krypton, Neon and Xenon, and all the most relevant aspects of these must be evaluated to choose the most suitable gas for our needs. The gas that best meets our requirements turned out to be Xenon. Specifically, thrust efficiency was chosen as the propulsive parameter to be maximized during our analysis. Using Xenon as a propellant gas, the optimization is performed by determining the optimal dimensions of the source (cylindrical in shape), the mass flow rate of the propellant, the intensity of the magnetic field and the electrical power generated by an RF antenna around the source. This analysis is conducted considering the technological limits imposed by the state of the art and by the size of the CubeSat that hosts REGULUS. The analysis is subsequently refined more and more until optimal values of $\eta_{max} = 7.39\%$ are obtained with $R = 0.03m$, $L = 0.1m$, $\dot{m} = 96 \times 10^{-9} kg/s$, $B_0 = 600 \times 10^{-4} T$ and $Pw = 40W$. When these results have been obtained, we proceed with an evaluation of how much the

limits imposed by the dimensions and technology have influenced the maximization of the thrust efficiency it is determined that the intensity of the magnetic field represents the most stringent limit to the propulsive performance of our engine .

Sommario

La propulsione elettrica rappresenta la nuova frontiera tecnologica della propulsione spaziale; sebbene si tratti di una tecnologia ancora in fase di sviluppo e con grosse limitazioni prestazionali, presenta in alcuni specifici casi degli aspetti che sono assolutamente vantaggiosi. La possibilità di generare spinta sfruttando energia elettrica è uno di questi: in orbita terrestre la radiazione solare è tale da fornire un costante approvvigionamento di energia che con i motori chimici non sarebbe possibile sfruttare. D'altro canto, il motore chimico rappresenta ancora oggi il metodo più efficace per un lanciatore di portare carichi in orbita, poiché la spinta di un motore elettrico non ha ancora raggiunto livelli tali da adempiere a questo compito. I propulsori elettrici si suddividono principalmente in due classi, propulsori con catodo e propulsori senza catodo. Il propulsore che verrà studiato in questa tesi appartiene alla categoria dei cathodeless thrusters, e più nello specifico si parla di Helicon Plasma Thrusters. Il nome di questi propulsori deriva dalla figura elicoidale che le particelle cariche disegnano con la loro traiettoria se immerse in un campo magnetico. Lo scopo di questa tesi sarà quello di ottimizzare un Helicon Plasma Thruster da 50W attraverso l'utilizzo del cosiddetto "Global Model", un codice scritto in linguaggio Matlab che descrive la fisica del plasma e successivamente determini le performance propulsive del motore stesso. Il Global Model permette di risolvere due equazioni differenziali del secondo ordine che sono rispettivamente l'equazione di bilancio di massa e l'equazione dell'energia. E' dalla soluzione di queste equazioni che diviene successivamente possibile, tramite un altro blocco di codice chiamato "Propulsion Model", determinare le caratteristiche propulsive del motore.

La nostra analisi si concentra dapprima sulla scelta del propellente più adatto ai nostri scopi. I gas più comunemente usati per la propulsione elettrica sono Argon, Krypton, Neon e Xenon, e di questi andranno valutati tutti gli aspetti più rilevanti per scegliere il gas più adatto alle nostre esigenze. Il gas che meglio soddisfa i nostri requisiti si è rivelato essere lo Xenon. Nello specifico, è stata scelta l'efficienza di spinta come parametro propulsivo da massimizzare durante la nostra analisi. Utilizzando lo Xenon come gas propellente, si precede con l'ottimizzazione determinando le ottimali dimensioni della sorgente (di forma cilindrica),la portata massica di propellente, l'intensità di campo magnetico e la potenza elettrica generata da un'antenna RF attorno alla sorgente. Si conduce questa analisi tenendo conto dei limiti tecnologici imposti dallo stato dell'arte e dalle dimensioni del CubeSat che ospita REGULUS. L'analisi viene successivamente raffinata sempre di più fino ad ottenere i valori ottimali di $\eta_{max} = 7.39\%$ con $R = 0.03m$, $L = 0.1m$, $\dot{m} = 96 \times 10^{-9} kg/s$,

$B_0 = 600 \times 10^{-4} T$ and $Pw = 40W$. Quando sono stati ottenuti questi risultati si procede con una valutazione di quanto i limiti imposti dalle dimensioni e dalla tecnologia abbiano influito sulla massimizzazione dell'efficienza di spinta s determina che l'intensità di campo magnetico rappresenta il limite più stringente alle performance propulsive del nostro propulsore.

Contents

List of Figures

List of Tables

Introduction

Cathodeless Thrusters

These thrusters are characterized by an exhaust that is totally free of electric charge, meaning that a neutralizing cathode for the expelled particles is not required. Such thrusters can be divided into "grid" and "magnetic nozzle" thrusters. The grid thruster involves the use of polarized grids thanks to which an electrostatic potential difference is imposed between the grids and the plasma itself: this ensures that an acceleration mechanism of the charged particles is guaranteed. In this type of thruster, the grids are polarized with alternating positive and negative potential, so that both the electrons (with a negative charge) and the ions (with a positive charge) composing the plasma are ejected out of the nozzle [9]. On the other hand, the magnetic nozzle thruster uses divergent magnetic field lines (which act in a similar way to De Laval physical nozzle) by converting the internal energy of the plasma into the kinetic energy of the particles ejected from the engine [1], [19]. For this type of thrusters, it is of fundamental importance that the plasma generated in the source has a high temperature and a high density, since the thrust generated by the engine strongly depends on the internal enthalpy of the plasma. It is possible to generate a plasma with these characteristics by irradiating the gas contained in the source with electromagnetic waves produced by an RF antenna: this process favors the generation of high-density plasma through the collision between neutral atoms and free electrons [9].

Typically, cathodeless thrusters have a structure that can be divided into three sections: the propellant storage and supply system, the plasma source and the acceleration zone. We describe the various sections one at a time: the storage and supply system are basically a tank from which the propellant is taken to be injected into the source through an injector. The source is made of a cylinder of dielectric material where the gas is injected with a certain flow rate, which is then irradiated with electromagnetic waves until plasma is obtained. The external walls of the source are surrounded by the RF antenna which permits to ionize the gas through electromagnetic waves. A magnetic field is also generated inside the source, using either electromagnets or permanent magnets: both configurations have advantages and disadvantages, for example the fact that the electromagnets require a constant current flow to be activated, whereas permanent magnets are typically heavier and generate a magnetic field that cannot be switched off when needed. The field of use of the thruster must always be taken in consideration, and from that decide which type

of magnet is the best to adopt [11]. The region of acceleration of the ejecta is instead formed by a so-called "magnetic nozzle", formed by the natural divergent attitude of the magnetic field lines, and is usually associated with a physical De Laval nozzle capable of generating propulsive thrust also for the gas that has not been ionized [17]. Focusing on the ionized part, the plasma exhaust can be divided into two distinct regions: the first will be defined by the region of space in which the charged particles follow a trajectory along the magnetic field lines, while the second part is delimited by the so-called *zone of detachment* and from this point on the particles will no longer follow the field lines but will continue along a rectilinear trajectory that runs parallel to the axis of the source. The moment in which the trajectory of the charged particles detaches from the field lines is of fundamental importance: in fact, if this were not the case, the particles would continue to follow the field lines, which according to Maxwell's laws would close on themselves, thus generating zero net thrust.

The presence of a magnetic field around the source therefore assumes a threefold function: it favors the diffusion of the electromagnetic waves through plasma in the source, it helps to confining the charged particles in a certain volume, keeping them away from the walls (with the double effect of thickening the charged particles and limiting losses due to collisions with the walls themselves) and allows to transform the thermal energy contained in the plasma of the source into axial kinetic energy and therefore into thrust. The presence of a magnetic field around the source therefore assumes a threefold function: it favors the diffusion of the electromagnetic waves through plasma in the source, it helps to confining the charged particles in a certain volume, keeping them away from the walls (with the double effect of thickening the charged particles and limiting losses due to collisions with the walls themselves) and allows to transform the thermal energy contained in the plasma of the source into axial kinetic energy and therefore into thrust. The presence of a magnetic field around the source therefore assumes a threefold function: it favors the diffusion of the electromagnetic waves through plasma in the source, it helps to confining the charged particles in a certain volume, keeping them away from the walls (with the double effect of thickening the charged particles and limiting losses due to collisions with the walls themselves) and allows to transform the thermal energy contained in the plasma of the source into axial kinetic energy and therefore into thrust. The presence of a magnetic field around the source therefore assumes a threefold function: it favors the diffusion of the electromagnetic waves through plasma in the source, it helps to confining the charged particles in a certain volume, keeping them away from the walls (with the double effect of thickening the charged particles and limiting losses due to collisions with the walls themselves) and allows to transform the thermal energy contained in the plasma of the source into axial kinetic energy and therefore into thrust [17], [9]. The cathodeless thrusters can be further subdivided according to the nature of the electromagnetic waves generated by the RF antenna: we are therefore talking about *Helicon Plasma Thrusters* (HPTs) and *Electron Cyclotron Resonance* (ECR), which are distinguished according to the frequency of the electromagnetic waves generate. Helicons' waves belong to the *whistler waves* or electromagnetic waves that propagate inside the plasma confined in a certain volume by the magnetic field. These waves, characterized by a frequency in the MHz order, transmit energy in a very efficient way to all the free electrons of the gas, guaranteeing a high number of collisions between these free electrons and the neutral gas particles, which are thus ionized. This excellent energy transmission turns out to be about three orders of magnitude higher than if only the energy transmitted by the collisions of the excited electrons were considered [2]. Speaking instead of the Electron Cyclotron Resonance, we have electromagnetic waves

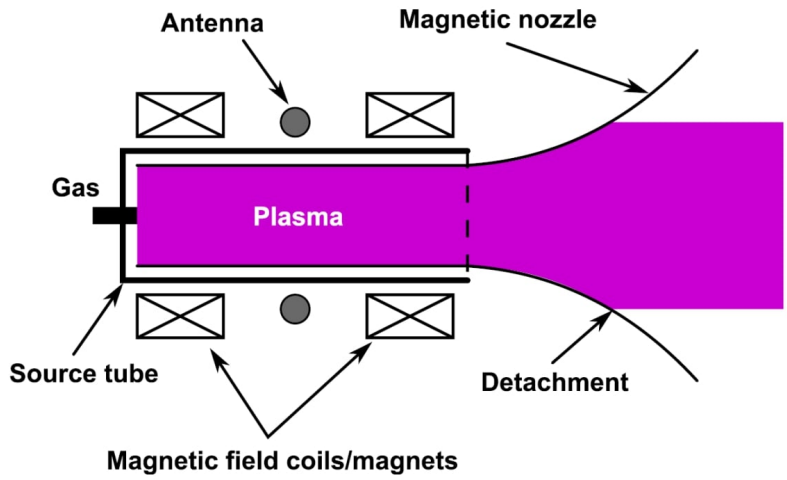

Figure 1: Scheme of a cathodeless Plasma Thruster

characterized by frequencies in the order of GHz, which have an efficiency of about 95% in energy transmission. Thanks to this high efficiency, the electrons reach a high thermal energy, which is then exploited to increase the collisions between electrons and neutral atoms generating a high density plasma [8].

Cathodeless thrusters present innumerable advantages: their components are not very complex and cheap, and the fact that they do not need a cathode to neutralize the exhaust guarantees a long life both for the component and for the engine itself. They also have a wide range of applicability: they can be used from microsatellites in low Earth orbit to interplanetary missions, which translates into a wide electrical power spectrum (from $\sim$ 20W to 200kW). They also offer the possibility of using various propellants, including Iodine [3] (stored in the solid state) and gases such as Argon and Xenon [20], alongside a wide range of possible mass flow rates. One of the major disadvantages in the use of cathodeless thrusters is the relatively low thrust efficiency, which usually does not exceed 20% [8]. Knowing this data, it is therefore easy to understand how the power supplied by the RF antenna is mainly used for the excitation of neutral atoms and in the neutralization of the ions, instead of being transformed into propulsive thrust. The ionization of neutral atoms takes place through various steps (which is the most effective method of ionizing an atom) but at the same time involves the formation of excited atoms in the intermediate steps. This process can lead to the de-excitation of the atoms before they have been ionized, or to the expulsion of the same atoms through the exhaust. In both cases, there is a loss of energy, which is in no way exploited to generate propulsive thrust. In addition to these phenomena, it has been noted that the number of ionizations inside the source far exceeds the number of electrons leaving the exhaust: this means that many plasma particles tend to be neutralized due to impacts with the walls, and the expenditure of energy becomes double that which would be strictly necessary to generate the same quantity of plasma [11].

Since the first research on a Helicon Plasma Thruster was presented in the 2000s (Boswell, Australian Space University) [7], many experiments have been conducted and many contributions have been given to the development of this technology, including *REGULUS*, developed by Technology for Innovation (T4i), a start-up associated with the University of Padua [17]. REGULUS is a 50W plasma thruster of the Helicon Plasma Thrusters family, developed to be placed on board small CubeSAT units. This specific engine will be the thesis topic to be developed in this draft.

Models for Cathodeless Thrusters

In order to develop a precise model of cathodeless thrusters, it is necessary to use numerical simulations that describe and allow us to fully understand the dynamics of the plasma. To ensure that the modeling is accurate, it is good to be able to integrate the following aspects into the simulation [5], [16]:

- Adequately model the coupling between electromagnetic waves and the plasma, and this strongly depends on the geometry of the magnetic field and on the parameters that characterize the plasma itself.
- Precisely describe the ionization of the propellant, all the reactions that take place between the particles and the diffusion of all the charged particles, which then define the steady state characteristics in the source.
- The expansion and acceleration of the propellant in the area of the magnetic nozzle.
- Modeling of the detachment criteria of plasma particles from magnetic field lines.

During the entire path of the gas, from the injection into the source to the discharge of the magnetic nozzle, the physics and characteristics of the plasma and the neutrals undergo significant variations: in the source the plasma has typical densities of $10^{-19}\mathrm{m}^{-3}$ while in the area of the magnetic nozzle the density is reduced to 10^{-14} m^{-3}. For this reason, different classes of algorithms are used for each different area of the engine.

Fluid codes:

They allow to calculate the characteristics of the plasma as a function of space and time, through the integration of the Magnetohydrodynamic (MHD) equations. These equations are meant to be used mainly in regions where the plasma assumes high densities [5], [16].

Particle Codes:

This type of code, on the other hand, allows the trajectories of the individual particles to be integrated and is particularly suitable for areas where the plasma is present in low densities [5], [16].

Hybrid Codes:

Finally, this kind of code is a hybrid between the other two codes mentioned above. It describes the motion of electrons through the Fluid Code and the dynamics of the ions through the Particle Codes [10].

In addition to these models, which provide precise and accurate results, analytical and semi-analytical models have also been developed. The rapid results that the latter can provide are useful for preliminary designs, to study the system as a whole and determine which phenomena are of mainly importance to define propulsive performance. In 2014 Lafleur proposed a semi-analytic model of a whole HPT, which included both a model for the source (based on the simplification and subsequent integration of the MHDs in a one-dimensional domain) and a model for the acceleration region (based on the hypothesis of an isothermal expansion of the plasma). Another *quasi one-dimensional* kinetic model, based on the evaluation and integration of the distribution function of ions and electrons, has been proposed by Martinez *et al.*, and has been simplified from Plaza *et al.* along with Lafleur *et al.* They also proposed an empirical model of the acceleration region, and this model aims to link the thrust generated by the propulsor to the final temperature of the electrons, through the derivation of an empirical constant. Fruchtmann *et al.* instead dealt with defining a model that describes the acceleration region, using a two-dimensional and semi-analytical model based on the strategy of separating the variables between their axial and radial components.

The latter model was revised and modified by Ahedo and Navarro-Cavallè who integrated this model with that of a two-dimensional nozzle, in order to create a tool that can efficiently simulate the steady state of the HPT. In this drafting a semi-analytical model written on Matlab code is used for the study of the thrusters, and this model is articulated in two main blocks: first block describes a model of the source (which includes the production of the plasma, the collisions of the particles and the diffusion of the same) and the second block describes the model of the acceleration region. The plasma source is modeled through a 0-dimensional Global Source Model (GSM) based on the description of the source as a single node characterized by the mass and energy balance entering and leaving the source itself. Contrary to the other models, this last one allows to describe the magnetic field no longer as paraxial but considering all the typical topological peculiarities of the magnetic fields produced by toroidal permanent magnets, as well as the presence of cusps within the source. The acceleration region is instead described by another code, which is written by adapting and combining the GSM model with the three models of the MN seen previously: the Lafleur model (LM) the Martinez-Sanchez model (MSM) and the Correyero Plaza model (CPM). In addition, various criteria are taken into consideration to define the region where the particles ejected from the exhaust detach from the magnetic field lines, and these are Olsen's criterion and Arefiev's criterion [12].

Thesis' structure and objective

This thesis work aims to optimize a REGULUS thruster, through computer simulations of the physics of the thruster, with the aid of precompiled Matlab code. This code requires the following quantities to be adopted as input variables: mass flow rate injected into the source, intensity of the magnetic field produced by the permanent magnets around the source, electrical power supplied to the plasma by the RF antenna, source length and source radius. The code allows to solve two differential equations describing respectively mass balance and energy balance in the source. Solutions provided by the code are continuous functions in time domain describing how the following quantities vary during simulation time interval: density of the neutral and charged species and electron temperature. Thanks to the final values that these quantities assume once the steady state is reached, it is possible to calculate the propulsive performance through another block of code, which returns the following quantities: specific impulse, thrust efficiency and propellant consumption.

–1–
Reference Models

In this chapter we will try to describe in more depth the nature of the equations that make up the two models used by our Matlab code. The models used is specifically the Global Model.

1.1 Global Model

This model describes in a simplified way what happens inside the source, taking into consideration both the neutral gas atoms and the plasma particles. Its main characteristic is that it is a 0-dimensional model: this means that the source domain will not be modelled to obtain a gradient of all the characteristic quantities describing the plasma, but rather to obtain such quantities averaged over the whole source domain. In other words, if we took as an example a variable such as the temperature of the electrons T_e, we will not obtain a function that describes the temperature of the electrons at a given point of the source, but we will obtain a function that describes the time variation of the average T_e of all the electrons in the source.

1.1.1 Hypotheses

As already mentioned above, the 0-dimensional model that is the Global Model is a combination and a simplification of other models describing plasma physics. To ensure that the Global Model represents physical phenomena as validly as other more complex models, it is due to list the hypotheses under which Global Model must operate:

- The magnetic field B produced by the permanent magnets has a cylindrical shape and it's axial; moreover, the effects of the magnetic field cusps are not considered, since these models are also used to study cases in which the source is surrounded by coiled electromagnets instead of permanent magnets.
- The ion's temperature is considered constant and is equal to the temperature of the neutral gas at the time of injection into the source.

- The transmission of power is assumed, but without defining a model. Therefore, in the Global Model a power deposition efficiency has been considered.
- At the edges of the sheath, the velocity of the ions equals the Bohm velocity (Bohm's criterion) [14].
- The diffusion of the plasma is modelled with the aid of the Langevin section [14].
- The ratios between the core plasma density and the sheath edge density are calculated using the heuristic parameters h_R and h_L [14], [13].
- For neutral particles, it is assumed that the nozzle is choked. A similar assumption is also adopted for the plasma: the magnetic Mach $m = v/u_B$ (where u_B is the Bohm velocity) in the throat is considered as equal to 1 [18].
- Given the assumption of ions at constant temperature, it is necessary to include a detachment criterion: the chosen criterion states that the ions detach from the magnetic field lines when the Larmor radius equals the local radius of the magnetic field flux tube [13].
- It is assumed that the electrons are present in the source according to a Maxwellian distribution.

1.1.2 Mass and Energy balances

As has been described in figure 1.1, in addition to the engine performance, the results obtained from the GM code block accurately describe what happens in the source in terms of density of the species present and temperature of the electrons T_e. Since the simplifications made through the hypotheses described above are valid, these parameters are sufficient to describe what happens in the source. To obtain these parameters, Matlab must solve two differential equations relating to the mass and energy balance, and this is what we will illustrate in the next paragraphs.

Mass Balance

There is a generic differential equation describing the mass balance in an exhaust chamber, which is as follows:

$$\frac{dn}{dt} = R_c - R_{wall} - R_{ex} + R_{in} \tag{1.1}$$

It is due to specify that all terms to the right of the equal have units of measure expressed in $[m^{-3}s^{-1}]$, and now these terms will be treated one by one:

1. The particles source-sink term related to the reactions taking place inside the source is described in the equation 1.2:

$$R_c = \sum_j n_e n_j K^k \tag{1.2}$$

Where n_j and n_e are respectively the density of the considered species and the density of the electrons and K^k is the reaction coefficient for the considered reaction. The term R_c considers from time to time all the particles of the various species (neutral, ions, excited particles) which are continuously formed and lost due to the reactions already described. Therefore, R_c can be positive or negative, depending on the considered reaction.

2. If an ion were to impact against the wall of the source, there would be a high probability that it would snatch an electron from the wall itself, and that as a result the ion would return to being a neutral particle. To include this eventuality in the calculations, the term describing these losses is introduced into the mass balance equation:

$$R_{wall} = \Gamma_{wall} \frac{A_{eff}}{V} \tag{1.3}$$

The term Γ_{wall} describing the ion flux (which is also equal to the electron flux) is calculated as:

$$\Gamma_{wall} = n_i v_i = n_i \sqrt{\frac{qT_e}{m_i}} \tag{1.4}$$

Where $v_i = u_B$ is the Bohm velocity of the ions while n_i and m_i are respectively the density of the ions and their atomic mass. In equation 1.3, A_{eff} is the effective area related to diffusion phenomena, which is calculated in equation XXX. The two components of this equation are nothing more than the two longitudinal and perpendicular components of the effective area and these components are calculated as seen from the equation 1.5.

$$A_{eff} = A_{||B} + A_{\perp B}$$

$$A_{||B} = h_L \beta_{avg} \pi R^2 \quad A_{\perp B} = 2 h_R \pi R L \tag{1.5}$$

The parameters present in this last equation, h_L, h_R and β_{avg} are defined in the section that describes the Diffusion Model.

3. The term representing the number of particles that are ejected out of the exhaust is described by:

$$R_{ex} = \frac{\dot{m}_n}{m_n} \frac{1}{V} + \Gamma_{ex} \frac{A_{sec}}{V} \tag{1.6}$$

The first term to the right of the equation describes the number of neutral particles leaving the source, considering the particle stream as isentropic and the nozzle as chocked. Since the plasma thruster is expected to operate in the vacuum of space, the chocked nozzle hypothesis always holds true [21]. The second addendum refers to the ions ejected from the exhaust, where the nozzle area at each point is calculated as: $A_{sec} = \pi R^2$. The flow of ions is instead described by:

$$\Gamma_{ex} = \beta_{avg} n_i h_L u_B \tag{1.7}$$

It is also assumed that the flow of electrons leaving the nozzle is equal to the number of electrons, to guarantee the quasi-neutrality of the plasma.

$$\Gamma_{ex,e} = \Gamma_{ex,i} \tag{1.8}$$

4. The particles that are injected into the source through the injector are represented by the term:

$$R_{in} = \frac{\Gamma_{in}}{V} \tag{1.9}$$

Where the term Γ_{in} represents the mass flow rate of neutral gas entering the source.

Energy Balance

The energy balance equation allows to determine the temperature of the electrons T_e, and this balance is expressed as written below:

$$\frac{d}{dt}(\frac{3}{2}n_e T_e) = P_{acq} - P_{lost} \tag{1.10}$$

The first term to the right of the equal represents the amount of energy that is absorbed by the gas and then transformed into plasma:

$$P_{acq} = \frac{P_{abs}}{qV} \tag{1.11}$$

Where the term P_{abs} is defined between the model inputs. The second term instead describes the energy loss defined by collisions with the walls, collisions with other particles and the material ejected from the exhaust:

$$P_{lost} = P_{wall} + P_{collision} + P_{exhaust} \tag{1.12}$$

Again, addends of equation 1.12 are analysed one by one. The power lost due to collisions with walls can be expressed as follows:

$$P_{wall} = \frac{\varepsilon_{wall}\Gamma_{wall}A_{eff}}{V} \tag{1.13}$$

Where Γ_{wall} is the same term that is described in the equations 1.4 and the term ε_{wall} represents the energy dispersed to the walls and is defined by the 1.14.

$$\varepsilon_{wall} = k_e T_e = \left(2.5 - ln\left(\sqrt{\frac{2\pi m_e}{m_{Ar}}}\right)\right) T_e \tag{1.14}$$

where the term k_e indicates the energy that is dispersed for each electron that is torn from the walls. The power loss given by collisions between two different species is calculated as indicated by the equation 1.15:

$$P_{collision} = \sum_j n_e n_{Ar,j} K^j_{Ar} \varepsilon^j_{Ar} \tag{1.15}$$

where the index j is used to indicate the species involved in the reaction. Finally, the power dissipated in the ejection of particles from the exhaust is expressed as follows:

$$P_{exhaust} = k_e T_e \frac{\Gamma_{ex,e} A_{sec}}{V} \tag{1.16}$$

Concerning the previous equation, we recall that the term $\Gamma_{ex,e}$ has already been defined in the equation 1.8.

1.1.3 Acceleration Model

This model allows to evaluate the propulsive performance of the engine. It is good to point out, as indeed it was anticipated in previous sections, how the hypothesis of isothermal ions makes it necessary to define a criterion for the detachment of these particles (positively charged). The detachment criterion considered in this case is the Lafleur criterion [13]. One of the most interesting propulsive parameters is thrust; it can be seen as the sum of two contributions, one of which is linked to the thrust generated by the neutral particles and the other generated by the charged particles that are expelled from the nozzle.

$$T = T_i + T_n \tag{1.17}$$

The contribution to the thrust that is given by the ions depends directly on the detachment criterion that is chosen [13]:

$$T_i = T_0 \left(\frac{M_{det}^2 + 1}{2M_{det}} \right) \tag{1.18}$$

In the previous equation, the term $T_0 = 2q\beta h_L n_i T_e A_{th}$ is the thrust that is generated by the charged particles leaving the source, while the second member, which depends on M_{det} represents the acceleration component due to the presence of the magnetic nozzle. To determine the detachment Mach number, the following equation must be solved [13]:

$$\frac{1}{2}(M_{det}^2 - 1) - ln(M_{det}) = ln\left(\frac{qB^2 R_{th}^2}{m_i T_\infty} \right) \tag{1.19}$$

which was obtained by integrating the momentum conservation equation of the charged particles. The integration extremes are represented respectively from the point where the particles leave the source (nozzle throat) to the point where the gyroradius of the charged particles equals the radius of the magnetic flux tube that composes the magnetic nozzle. The thrust component produced by the neutral particles is calculated using the classic form of the chocked nozzle crossed by an isentropic flow, which we remember to be [21]:

$$T_n = \dot{m}_n u_n + p_{exit} A_{exit} \tag{1.20}$$

Now that it is known how both the thrust components are calculated, as well as the total thrust value, it is possible to derive another important propulsive parameter, which is the

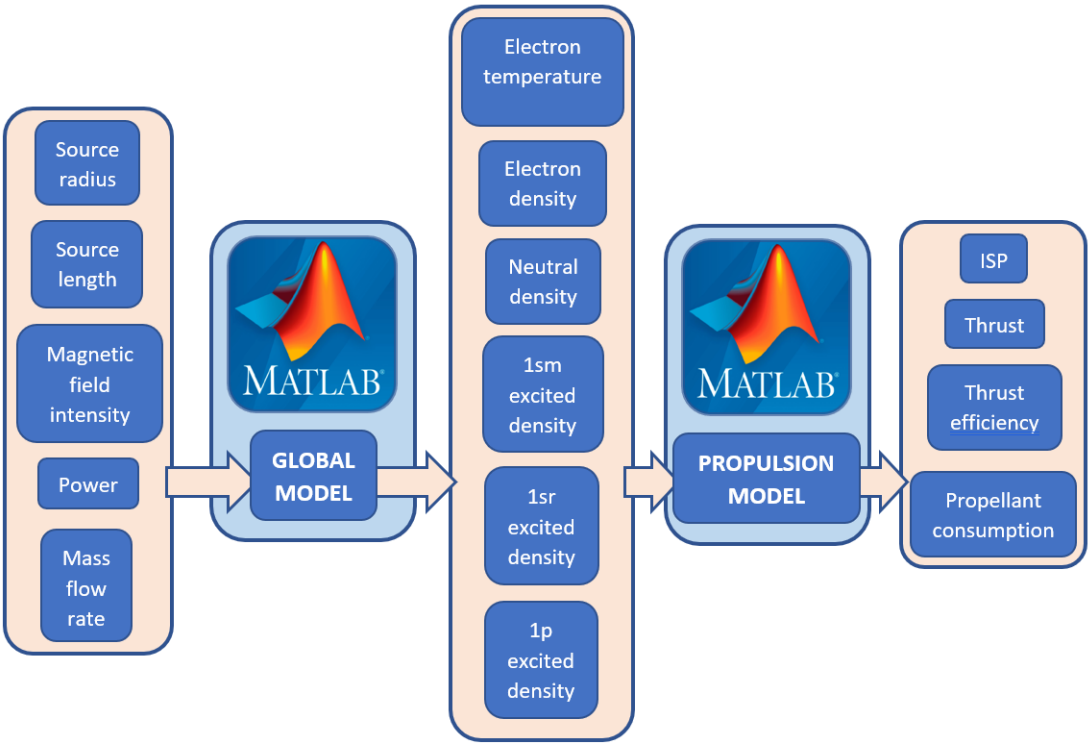

Figure 1.1: *Scheme of Inputs and Outputs of the Model*

specific impulse. It helps us define how efficiently our engine uses propellant to generate thrust.

$$Isp = \frac{T}{w_{tot} g} \tag{1.21}$$

Since the thrust efficiency η will be one of the parameters that occur most often within this draft, we report below a brief description of the same, defined as the ratio between the kinetic energy of the particles ejected form the engine and the electrical energy supplied to the source Pw, as we can see in equation 1.22:

$$\eta = \frac{Isp \times Thrust \times g}{2Pw} \tag{1.22}$$

1.1.4 Inputs and outputs of the model

The Global Model, as previously mentioned, outputs the various quantities that characterize the plasma in the source and through another block of code it is possible to determine the propulsive performance of the entire engine such as thrust, specific impulse and thrust efficiency. In figure 1.1 we see a graphical representation of the variables entering the code and in the blocks with red background we see the variables that are presented on the screen at the end of each solution cycle.

Reactions

In this section we will look more deeply into the reactions that are considered by the block of code called the Diffusion Model. In this example, the gas considered is Argon, but in the continuation of the drafting we will analyse all the possible gases that could be used as propellants. It should also be specified that this model does not take in consideration the collisions between heavy particles and electrons, but only describes the collisions between neutral gas atoms and electrons. The reactions considered are summarized in table 1.1.

Reaction	**Name**	**Threshold Energy [eV]**
$Ar + e \rightarrow Ar + e$	Elastic Collision	$\epsilon_{Ar}^{en} = (3m_e/m_{Ar})T_e$
$Ar + e \rightarrow Ar^* + e$	Excitation	$\epsilon_{Ar}^{elec} = 11.55$
$Ar + e \rightarrow Ar^+ + 2e$	Ionization	$\epsilon_{Ar}^{ion} = 15.76$

Table 1.1: List of reactions considered and threshold energies related to them [14]

In table 1.2 instead, the values of the reaction constants relative to table 1.1 will be defined:

Reaction	**Expression**
Elastic Collision	$K_{Ar}^{en} = 2.336 \times 10^{-14} T_e^{1.609} exp(0.0618(lnT_e)^2 - 0.1171(lnT_e)^3)$
Excitation	$K_{Ar}^{elec} = 5.02 \times 10^{-15} T_e^{0.74} exp(-11.56/T_e)$
Ionization	$K_{Ar}^{ion} = 2.34 \times 10^{-14} T_e^{0.59} exp(-17.8/T_e)$

Table 1.2: List of reactions coefficients [14]

Diffusion Model

The diffusion of ions and electrons inside the source is closely related to the way in which these particles, thanks to the action of the magnetic field, move along the axial and radial directions. As has already been mentioned among the Global Model hypotheses, the block of code describing the Diffusion Model uses the concept of the Langevin section [14]. The so-called Langevin Scattering, correlated with the elastic collision reactions of the electrons, allowing to calculate the mean free path of the electrons and consequently to calculate the collision frequency of the particles. Taking again Argon as the example gas,

it is possible to define the Langevin section as follows:

$$\sigma_i = -2.95 \times 10^{-19}\sqrt{\frac{3}{2}T_\infty} + 10.65 \times 10^{-19} - 2 \times 10^{-19}\sqrt{\frac{3}{2}T_\infty} + 7.8 \times 10^{-19} \tag{1.23}$$

In equation 1.23, T_∞ represents the temperature of the neutral gas. As we have already anticipated in the list of hypotheses, it is assumed that the temperature of the ions is equal to the initial temperature of the neutral gas at every instant: therefore, T_∞ also represents the temperature of the ions. Now that the value of the Langevin section is known, the mean free path of the electrons will be:

$$\lambda_i = \frac{1}{(\sum_j n_i)\sigma_i} \tag{1.24}$$

And consequently, the collision frequency between the ions can be expressed as:

$$\nu_i = \frac{v_{th}}{\lambda_i} \tag{1.25}$$

Where the term $v_{th} = \sqrt{\frac{8k_BT_\infty}{\pi m}}$ represents the thermal velocity of the electrons (while instead k_B is Boltzmann's constant). The collision frequency of the electrons is instead defined by the following formula:

$$\nu_e = \sum_j n_n K^j \tag{1.26}$$

Here instead, the term n_n represents the density of the neutral particles and the term K^j indicates the generic reaction coefficient, already described in the previous paragraphs.

$$D_{i||} = \frac{k_BT_\infty}{m_i\nu_i} \quad D_{e||} = \frac{qT_e}{m_e\nu_e}$$

The mobility coefficient $\mu_{||}$ and the diffusion coefficients $D_{||}$ along the axial direction of the magnetic field can be calculated for both electrons and ions as a function of the collision's frequencies seen in equations 1.25 and 1.26 [14]. We see them written below:

$$\mu_{i||} = \frac{q}{m_i\upsilon_i} \quad \mu_{e||} = \frac{q}{m_e\upsilon_e} \tag{1.27}$$

In these formulas it is good to pay attention to the fact that the temperature of the electrons T_e is expressed in $[eV]$ while the temperature of the ions T_i is expressed in $[K]$. From this difference in units of measure it is immediately understandable the presence of two different terms in the numerator of the two diffusion coefficients. Knowing these parameters, we can now calculate the same diffusion and mobility coefficients, this time along the direction perpendicular to the magnetic field lines, making use of the so-called

magnetic factor $f = \frac{1}{1+\left(\frac{\omega}{\nu}\right)^2}$,which in this case will be the same for both ions and electrons. The following expressions are obtained:

$$D_\perp = D_{||} f \quad \mu_\perp = \mu_{||} f \tag{1.28}$$

With the coefficients just calculated, the parameters of ambipolar scattering in the direction parallel and perpendicular to the magnetic field lines can finally be calculated. The ambipolar coefficient along the direction parallel to the field lines is obtained from the equation 1.29. While for the ambipolar coefficient in the direction perpendicular to the field lines two formulations are possible, expressed as a function of the magnetic field intensity, they are reported in the two equation 1.30 (respectively for low and high B) [14],) [6].

$$D_{a||} = \frac{\mu_{i||} D_{e||} + \mu_{e||} D_{i||}}{\mu_{i||} + \mu_{e||}} \tag{1.29}$$

$$D_{a\perp 1} = \frac{\mu_{\perp|} D_{e\perp} + \mu_{e\perp} D_{i\perp}}{\mu_{i\perp} + \mu_{e\perp}} \quad D_{a\perp 2} = \mu_{1\perp} T_e \tag{1.30}$$

The resulting coefficient of the perpendicular component will be a combination of the two transverse coefficients described in the following equation:

$$D_{RT} = exp((1-\lambda) log(D_{a\perp 1}) + \lambda log(D_{a\perp 2})) \tag{1.31}$$

Where λ is, in this case, the coefficient of the weights [15] and is set equal to 0.9. The ambipolar coefficients consider the diffusion phenomena which, due to the ambipolar electric field that develops in the plasma, tend to keep the plasma neutral. These parameters allow to obtain the two heuristic ratios between the densities that exist between the heart of the source and its walls, and these parameters are respectively h_L and h_R [13], [14].

$$h_L = \frac{0.86}{\sqrt{3 + \frac{L}{2\lambda_i} + (\frac{0.86 L u_B}{\pi D_a})^2}} \quad h_R = \frac{0.86}{\sqrt{4 + \frac{R}{\lambda_i} + (\frac{0.8 R u_B}{2.045 J_1 D_{RT}})^2}}$$

$$\beta_{avg} = \frac{1}{7(1 - h_R^{\frac{1}{6}})} \{[(1 - h_R^{\frac{1}{6}}) - 1]^7 + 1\} \tag{1.32}$$

Where the parameter β_{avg} represents the mean of the plasma density in the radial direction [13].

–2–
Preliminary Analysis

2.1 Evaluation of propulsive performances for each gas

The first challenge to face for the development of a space thruster is represented by the choice of the propellant. The most common propellant for electric propulsion are noble gases such as Argon, Krypton, Neon and Xenon; the task of the author of this thesis is to choose the gaseous propellant that presents the best propulsive performances, conducting a graphical analysis based on data obtained from Matlab simulations. Once the propellant gas has been chosen, only that gas will be used to proceed with subsequent thruster optimization analyses. It is good to mention the existence of a prototype of the REGULUS thruster, an HPT with a power of about 150W, which uses Xenon as a propellant gase [17].

2.1.1 Input parameters to the code

As already seen in figure 1.1, the Matlab code displays the following eight parameters on the command window as results of the simulations:

- Electron temperature
- Electron density
- Ionization ratio
- Neutral density
- Thrust
- Specific Impulse
- Thrust efficency ratio
- Propellant utilization efficency

Figure 2.1: *REGULUS Thruster*

These parameters are calculated within the "main" code which includes Global Model and Propulsion Model. At the "main" code, the following six parameters are supplied as inputs:

- Propellant gas
- Electrical Power
- Magnetic field intensity
- Mass flow rate
- Source radius
- Source length

These input parameters are briefly described in the following lines:

1. Propellant gas

   The Global Model is written in a Matlab code document called "main" and is supplied together with another Matlab document folder called "gas_data", from which the "main" imports the data related to each propellant gas to be used. Specifically, this folder contains four files that indicate all the parameters necessary for the “main” code to perform the calculations with all four possible gases to be used as propellants. These four gases are listed below:

   - Argon
   - Krypton
   - Neon
   - Xenon

   In line 24 of the "main" code it is possible to type the name of the gas to be used in the simulation (figure 2.2) to ensure that the "main" code knows from which file in the "gas_data" folder to import the data.

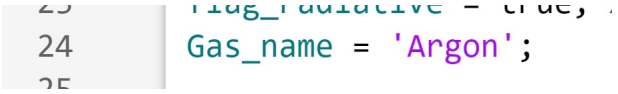

Figure 2.2: *Line 24 of "main", where Gas_name is to be selected*

2. Electrical power

   REGULUS is mounted on board a satellite which generates electric power with the aid of solar panels mounted on its surface. It is understandable that due to the small size of the satellite, the electrical power generated will have upper limits, which in

our case are around a value of 50 W [17]. Furthermore, during the transmission of energy from the solar panel up inside the neutral gas in the source, an efficiency factor around $\eta = 0.8$ was observed. It can therefore be written:

$$P_{gas} = \eta P_{electrical} \tag{2.1}$$

As a result, the 2.1 equation gives about $40W$ of power supplied to the neutral gas and plasma in the source. This power input is written by the user himself at line 61 of the "main" code, as we see in figure 2.3.

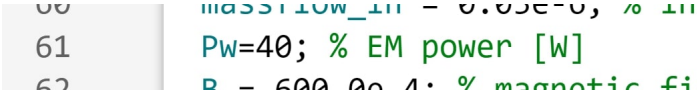

Figure 2.3: *Line 61 of "main", where Pw value is to be selected*

3. Magnetic field intensity

   As we have already described in the introduction to this draft, REGULUS mounts around the source two toroidal-shaped permanent magnets with a rectangular section. The thruster is housed in a case with dimensions of 1.5 CubeSat units and the remaining part of the avionics must also find accommodation inside the same case. Given these stringent volume limits, it is possible to define from the outset the dimensions of these magnets and consequently the intensity of the magnetic field generated by them. The magnetic field intensity obtained is around 600×10^{-4} Tesla and in the "main" this datum can be set in line 62 of the code:

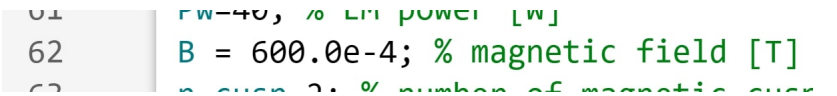

Figure 2.4: *Line 62 of "main", where Magnetic Field Intensity value is to be selected*

4. Propellant mass flow rate

   To define the propellant mass flow rate value, it is first necessary to carry out an analysis of the relationship between the mass of an electric propulsion unit and its specific impulse. The relationship between these two quantities is represented in figure 2.5, and it is good to know that this curve, having a positive inflection trend and with the presence of a minimum, is an exclusive characteristic of electric propulsion systems.

   The resulting curve indicated in figure 2.5 with $\Delta m + m_p$ is clearly the sum of the two contributions Δm and m_p which on the graph are indicated by the two dotted lines: the contribution Δm represents the mass of propellant, while the contribution m_p denotes the mass of the power unit of the satellite. We describe these two contributions in the following lines in more detail:

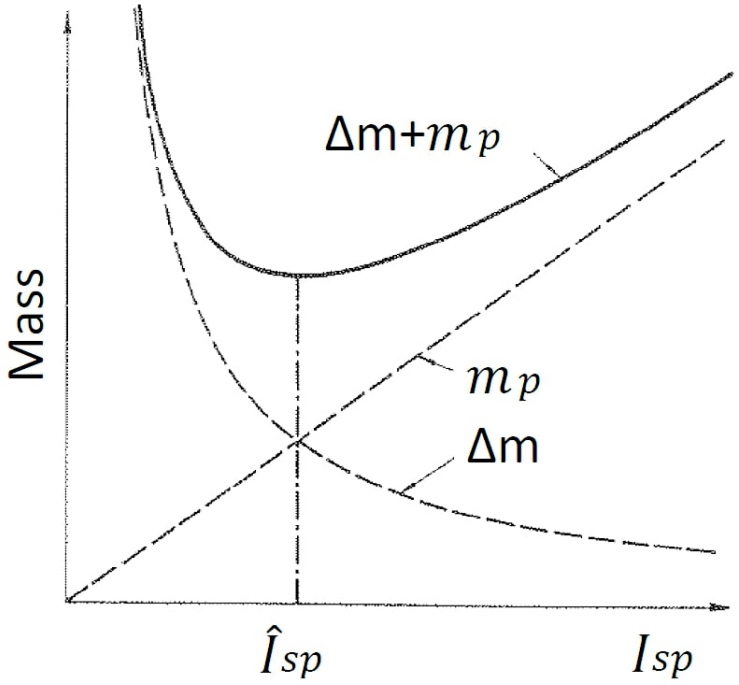

Figure 2.5: *Isp in function of mass contributes* Δm *and* m_p

- **Propellant mass**

  More precisely, Δm represents the trend of the propellant mass as a function of time, and is expressed according to the equation 2.2:

$$\Delta m = \dot{m}\Delta t = \frac{T\Delta t}{g_0 Isp} \tag{2.2}$$

  Note how this expression is directly proportional to the term $\dot{m}$ which expresses the propellant mass flow rate.

- **Power supply unit mass**

  The second contribution describes the mass of the power unit (which on an electric propulsion unit represents the most significant contribution to the total mass) as directly proportional to the electrical power generated. We can describe the relationship between m_p and the electric power P in equation 2.3:

$$m_p = \alpha P = \alpha \frac{\dot{m} v_e^2}{2\eta} = \frac{\alpha g_0 T Isp}{2\eta} \tag{2.3}$$

  Note how the term $\dot{m}$ appears here too, expressing the mass flow rate. At the point of the curve which represents the minimum total mass, an optimal

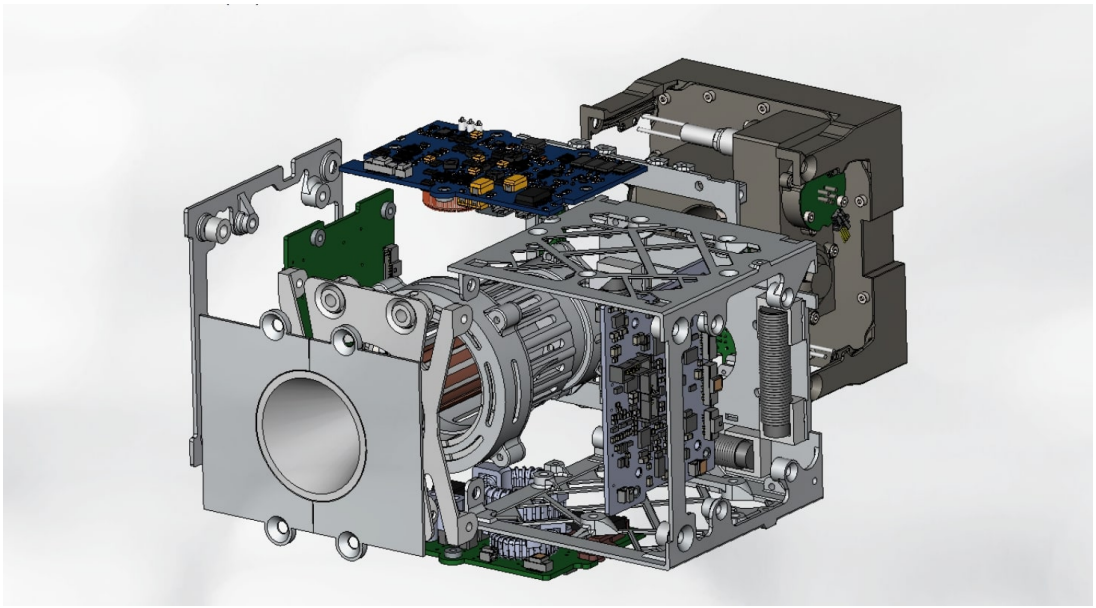

Figure 2.6: *Exploded view of REGULUS plasma thruster*

specific impulse value is defined, called $\hat{I}sp$. This value is expressed as follows:

$$\hat{Isp} = \frac{1}{g_0}\sqrt{\frac{2\eta\Delta t}{\alpha}} \tag{2.4}$$

Returning to the value of $\dot{m}$, we note that there is a minimum total mass value, which we know from depends on the two contributions Δm and m_p seen in figure 2.5. Since both contributions depend on the value of $\dot{m}$, we can conclude that, for a given thruster, exists a value of $\dot{m}$ which defines a minimum total mass, and consequently an optimal specific impulse $\hat{I}sp$. Plasma thrusters are designed to have burning times Δt in the order of months and, given the small size of the satellite under examination, only small masses of propellant Δm can be carried onboard. Since the mass flow rate can be expressed as $\dot{m} = \frac{\Delta m}{\Delta t}$ it is clear that, given the orders of magnitude of the numerator and denominator, the mass flow rate assumes very small values. Therefore, it becomes important to have very precise control over this parameter, and this is achieved by adopting suitable flow regulation valves. Based on simulations performed on the previous REGULUS version, a mass flow rate value of $30 \times 10^{-9}\ kg/s$, written in line 60 of the "main" code, is adopted for the preliminary analyses.

5. Source length

   As we can see from the exploded view in figure 2.6, the maximum length of the source is limited by the size of the single CubeSat unit in which the same source must be contained. Since the side dimension of a CubeSat unit is standardized at

$0.1m$ we can impose this value on the length of the source, at line 53 of the "main" code (figure 2.7).

```
51  % Geometry
52  R  = 0.02; % discharge radius [m]
53  L = 0.1; %  discharge length [m]
```

Figure 2.7: *Block of code relative to source's geometry*

Before proceeding with the description of the output parameters of the Matlab code it is necessary to make a clarification: once the propellant gas to be used in the simulation has been chosen, all the input parameters mentioned above are considered constant for the entire duration of the simulation, made exception for the electrical power. Contrary to all the other quantities, the electric power is not modelled as a step function (meaning that its value is zero up to an instant before the start of the simulation and from the following instant constantly equal to the final value), but follows an exponential law which starts from zero at the initial instant and tends asymptotically to the final value which is imposed at line 61 of the code. This exponential law is described in the equation below:

$$P_{absorbed} = Pw/q/V\left(1 - e^{-t/0.0001}\right) \tag{2.5}$$

Focusing on the second factor of the multiplication, which is the exponential function, we can observe how it is represented in the graph in figure 2.8:

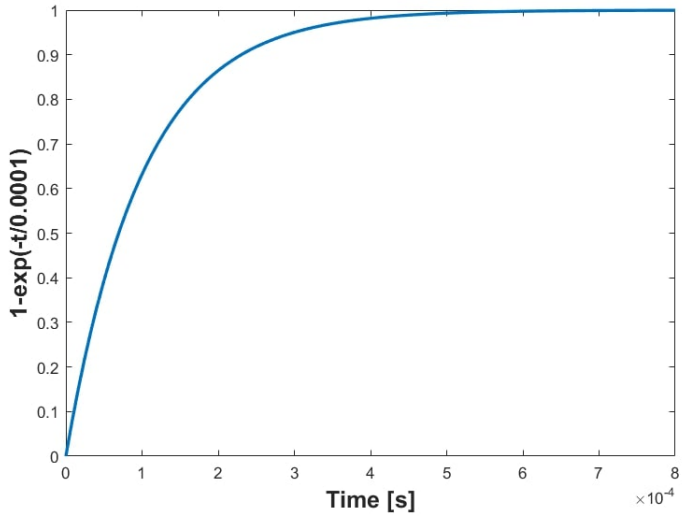

Figure 2.8: *Graph of exponential function in equation 2.5*

We note that this function reaches the final value in a time interval lower than $10^{-3}s$. Therefore, if compared with the entire duration of the simulation (which in our case remains fixed at $4s$) the power trend can also be traced back, with good approximation, to a step function. The need to define the trend of the absorbed power in his way derives from the desire to avoid the divergence of the solution of the energy equation. As we know, the energy equation is nothing more than a second order differential equation; as such, the convergence of its solution will strongly depend on the initial conditions that are imposed. A step modelling of the power trend could not guarantee an adequate convergence of the solution and for this reason it was decided to adopt the form described by the equation 2.5. This form guarantees a much more stable behaviour to the solution of the energy equation.

2.2 Results presented on screen

Once the parameters described in the paragraph above have been entered, it is possible to launch the simulation in Matlab. After some seconds (the resolution time depends on the initial parameters entered) Matlab returns two results to the screen: one appears in a new window, representing the electron temperature and density trends of species present in the source over time (figure 2.9) and another in the command window, where the most relevant parameters are presented at the end of the simulation together with the resulting propulsive parameters (figure 2.10). The two simulation's results are described in more detail below.

1. **Temperature and density of present species**

   The graphs shown on the screen describe the following parameters as a function of time:

   - n_{gs} defines the density of neutral gas in the source
   - n_{1sm} defines the density of atoms in the source with electrons excited at the $1s$ orbital that are metastable
   - n_{1sr} defines the density of atoms in the source with electrons excited to the $1s$ orbital that are resonant
   - n_{2p} defines the density of atoms in the source with electrons excited at the $2p$ orbital
   - n_e defines the electron density in the source
   - T_e defines the temperature of the electrons in the source

   These graphs all show the time variable $[s]$ along the X-axis, and the time interval represented is equal to the duration of the simulation, which in this case is $4s$. Note in figure that this value does not appear on the abscissa axis, due to the decision to adopt the logarithmic scale to represent this quantity. The duration

of the simulation is chosen to ensure that all the values could reach the so-called steady state, which is the condition whereby the values remain constant over time from a certain instant onward. The graphs in figure 2.9 show that this condition has been reached, since after a given instant of time the curves show a flat trend until the end of the simulation. If this does not occur, it is advisable to increase the simulation time so that this steady state condition occurs anytime. In this draft, for all the conducted analyses, the simulation time equal to $t = 4s$ was always sufficient for all quantities to reach the steady state.

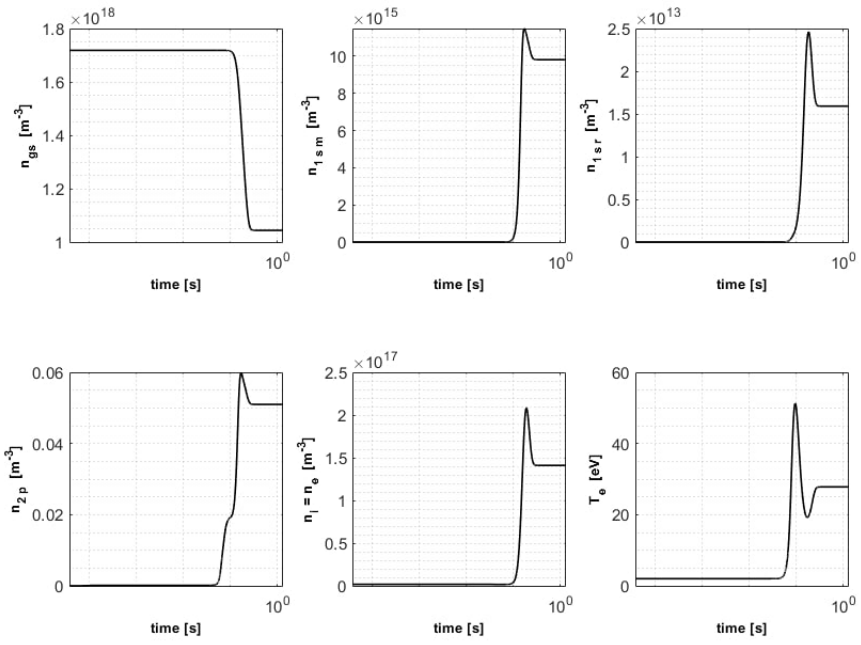

Figure 2.9: *Graphs presented in new window*

2. **Steady state parameters and propulsive figures of merit**

   The result appearing in the command window, on the other hand, presents the following values on the screen:

   - Steady state temperature of the electrons [eV]
   - Steady state density of electrons [$m^{-}3$]
   - Initial temperature of the neutral gas [K]
   - Steady state ionization ratio [-]
   - Steady state neutral pressure [Pa]
   - Thrust [mN]

- Specific impulse [s]
- Thrust efficiency [-]
- Propellant utilization efficiency [-]
- Mass flow rate [mg/s]

The propulsive parameters (*Thrust*, *Isp*, *Thrust Efficiency*, *Propellant Utilization Efficiency*) are calculated from a second block of code using the steady state parameters as input.

```
Te = 27.80 eV
ne = 1.41e+17 m^-3
T = 400 K
ionization_ratio = 0.12
neutral pressure = 0.01 Pa
Thrust = 0.4 mN
Isp = 1278 s
thruster efficiency = 0.05
propellant utilization = 0.39
mass flow rate = 0.03 mg/s
fx >>
```

Figure 2.10: *Parameters presented in command window*

Now that the code has been described exhaustively, let's proceed with the generation of graphs that help the reader to better understand how the steady state parameters and propulsive figures of merit vary at the variation of the different input parameters.

2.3 Trends of the output parameters at variation of a single input parameter

To have the broadest possible view on the operation of the plasma thruster, it was decided to produce graphs that allow to study the trends of all the parameters in the "main" output as a single input parameter varies, while the other parameters are kept constant. We summarize in the following lines the selected values of all the input parameters:

- $\dot{m} = 30 \times 10^{-9} kg/s$
- Magnetic Field Intensity = $600 \times 10^{-4}\ T$
- $Pw = 50\ W$
- $R = 0.02\ m$
- $L = 0.1\ m$

2.3.1 Mass Flow Rate

Matlab's "linspace" function allows us to generate a vector with a number of elements equal to the number of iterations we prefer (imputable as "n_iter" in line 49 in figure **??**). We note in line 51 of the code how the extremes of this vector are defined: the lower extreme will have a value of 0.1 times the pre-selected value of mass flow rate, while the upper extreme will have a value of 10 times the pre-selected valure of mass flow rate. The interval of two orders of magnitude between the final and initial values is chosen arbitrarily by the student; it is believed that such a wide interval is sufficient to sweep many of the most interesting values for the considered quantities ($\dot{m}$ in this case). For each single mass flow value defined with "linspace", a simulation is performed and the output data from the code is saved in vectors ready to be exported for further analyses. This procedure is carried out for all gases (Argon, Krypton, Neon and Xenon), to obtain the propulsive performance trends as the mass flow rate varies for each of the possible propellant gases. Once all the data has been saved, proceed by comparing the curves obtained on the same graphs, as we can see in figure 2.11. With reference to the graph

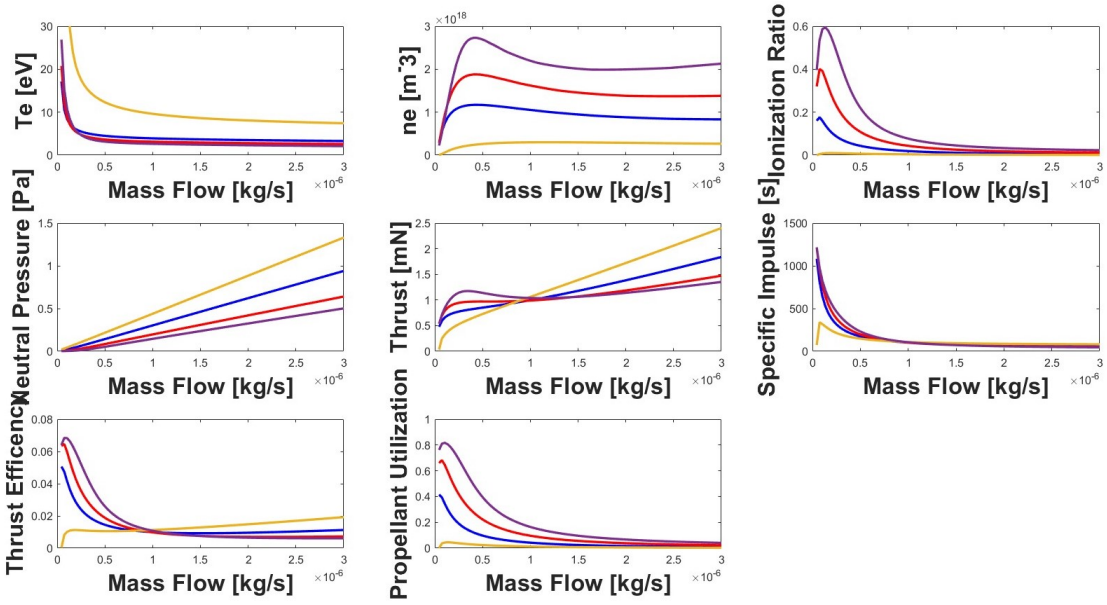

Figure 2.11: *Output parameters in function of $\dot{m}$*

above, we can make the following observations:

- The trends of the curves of all the parameters described as $\dot{m}$ vary are also similar among the different gases considered.
- In some cases, the curves tend to be more detached, while in other cases they can even intersect. Let us see, for example, how the trends differ for a mass flow rate value of $100 \times 10^{-9}\ kg/s$: if our goal is to have the maximum plasma density in the source (observe the graph of n_e) it is clear that using Xenon as a propellant gas

would have clear advantages over all the others, but if our goal were to maximize thrust or thrust efficiency, we note that, for the same mass flow rate, a different propellant gas would have very little influence.

- The curves relating to electron density, ionization ratio, thrust, thrust efficiency and propellant utilization efficiency all have local maxima: this means that, all other input parameters being equal, there is a certain mass flow value such that any one of these parameters can be maximized.

2.3.2 Magnetic field intensity

The procedure is similar to that relating to the mass flow: a preselected value of magnetic field intensity ($600 \times 10^{-4}\ T$) is defined and the "linspace" function generates a vector with extremes$[0.1 \times 600T, 10 \times 600T]$. An iterative cycle is then defined in Matlab which allows to have in line 62 input one element at a time of the new magnetic field intensity vector. The iterative cycle is repeated for all four possible gases to be used, and the resulting output data is again saved and subsequently analysed. The following graphs are obtained:

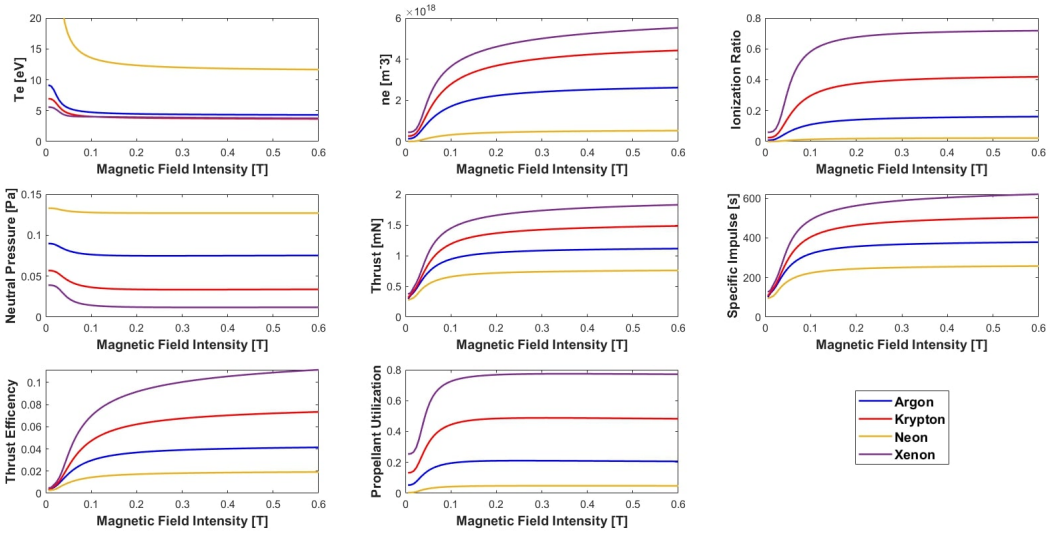

Figure 2.12: *Output parameters in function of Magnetic Field Intensity*

Referring to the graphs in figure 2.12 we can observe the following aspects:

- The curves are all clearly distinct from each other (except for very low values of magnetic field intensity values) and this suggests that as the propellant gas used varies, the characteristics of the plasma and the propulsive performance will tend to undergo variations. For example, for a magnetic field of $0.5T$ we can see that the specific impulse we would obtain if we used Neon as a propellant gas is around $200s$ while, if we had used Xenon, we would have generated a specific impulse of almost $600s$.

- The curves all show a monotonic trend without any relevant maxima, and this suggests the non-existence of an optimal value of magnetic field intensity that maximizes propulsive performance.

- The trends of the propulsive performance graphs are almost all monotonous increasing. Note how these curves present a first part in which, up to a certain point, propulsive performance also increases as the intensity of the magnetic field increases. From a certain point on, however, an increase in magnetic field intensity does not produce significant changes in propulsive performance.

2.3.3 Electrical power

The chosen value of electrical power supplied will be $50W$ while the vector generated with "linspace" will again have the extremes defined as $[0.1 \times 50W, 10 \times 50W]$. The iterative cycle is performed on the electrical power vector and the following graphs are obtained for different propellants. We deduce from figure 2.13 the following characteristics:

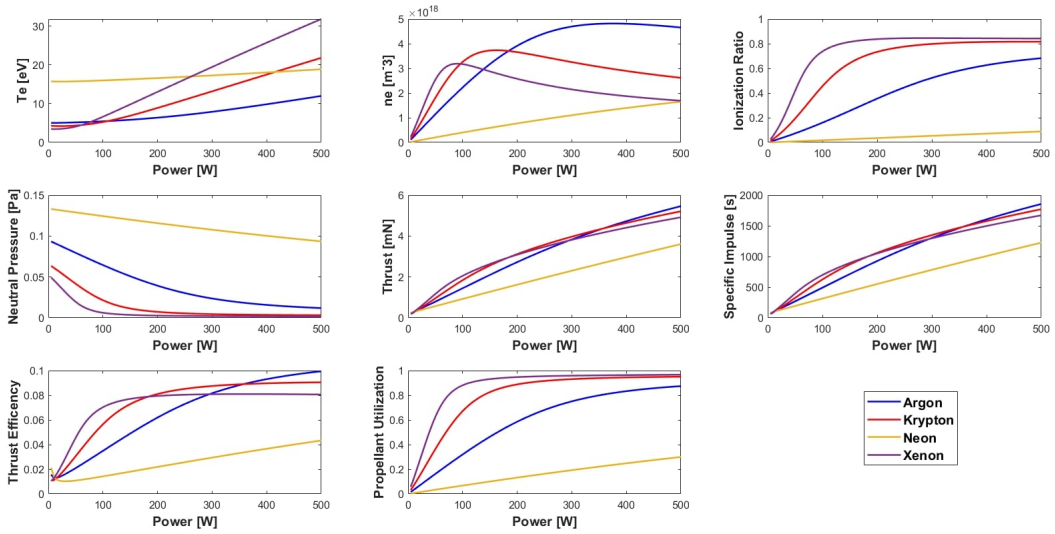

Figure 2.13: *Output parameters in function of Pw*

- The trends in the graphs do not have a uniform trend for all considered gases and the curves often tend to intersect each other; in this case it is less immediate to define which propellant gas determines the best propulsive performances.

- The presence of the peak in the n_e electron density curve relating to Xenon, Krypton and Argon is of considerable interest. This trend deserves a more accurate analysis that we will not deal with in this draft.

- The propulsive performance curves almost all show an increasing monotonic trend: the specific impulse and thrust values tend to increase as the electrical power

supplied increases, while it is noted that the values of thrust efficiency and propellant utilization efficiency reach a saturation beyond which there are no increases in performance.

2.3.4 Source Radius

The chosen source radius value is 0.02 m, but this time the endpoints of the vector used for the iterations are defined differently: the "linspace" function is set to generate a vector having endpoints $[0.1 \times 0.02m, 6 \times 0.02m]$. The reason for this different definition will be explained later in the following comments. Proceeding with the iterations on the elements of the vector containing all the possible source radii, always for each possible propellant gas, the underlying graphs are obtained. From figure 2.14 we can observe that:

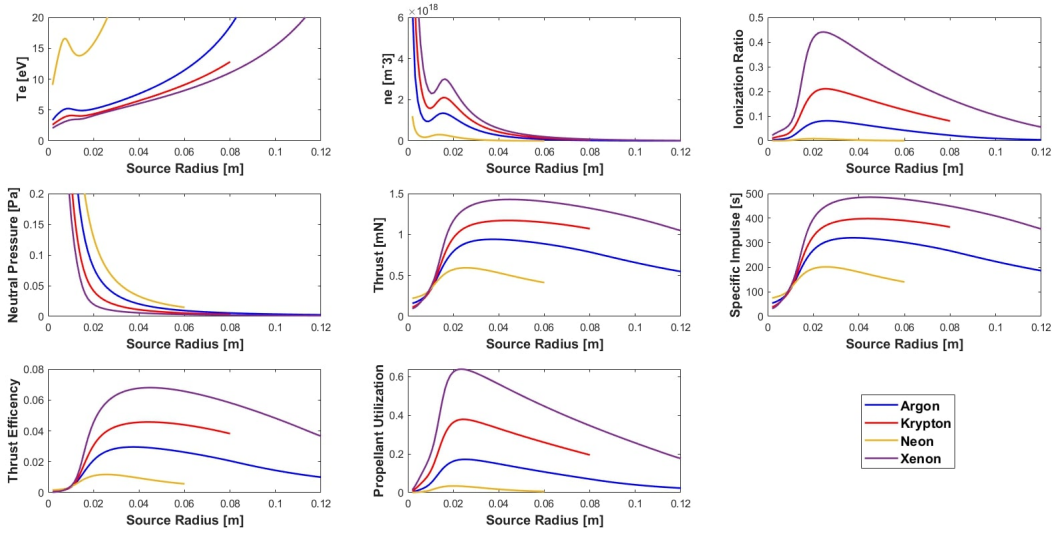

Figure 2.14: *Output parameters in function of source radius*

- The curves sometimes remain quite distinct from each other along the entire interval considered, while sometimes the curves tend to intersect for short stretches. As we have already seen for mass flow, for the values of source radius where the curves intersect, the choice of one propellant gas rather than another will have a reduced influence on propulsive performance. On the other hand, for sections where the curves are quite distinct, the propulsive performance will be more markedly influenced by the choice of propellant gas.
- The propulsive performance graphs all have an appreciable maximum point, and this indicates that, for a given propulsive figure of merit, there is an optimal radius for maximizing it (all other input parameters being equal).
- Unlike $\dot{m}$, Pw and $Magnetic\ field\ Intesity$ seen previously, the graphs of the different propellant gases have not been represented along the same range of values

(note the brevity of the Krypton and Xenon curves). This is due to an intrinsic feature of the Matlab code: as we have already mentioned, the Global Model includes two second order differential equations and the stability of their solution strongly depends on the initial conditions that are imposed; some source radius values do not guarantee adequate stability to the solution of the differential equation, and therefore the data obtained are not considered valid for making a clear comparison between the performance of the various gases. This is the reason why the vector of source radius generated with the "linspace" function has the extremes defined in a different way compared to all the other vectors seen previously.

2.3.5 Source Length

The chosen source length value is $0.1m$, and the extremes of the vector generated by the "linspace" function this time are $[0.1 \times 0.1m,\ 10 \times 0.1m]$. Following the iterative cycles, performed for each propellant gas, we obtain the underlying graphs. From the graphs in

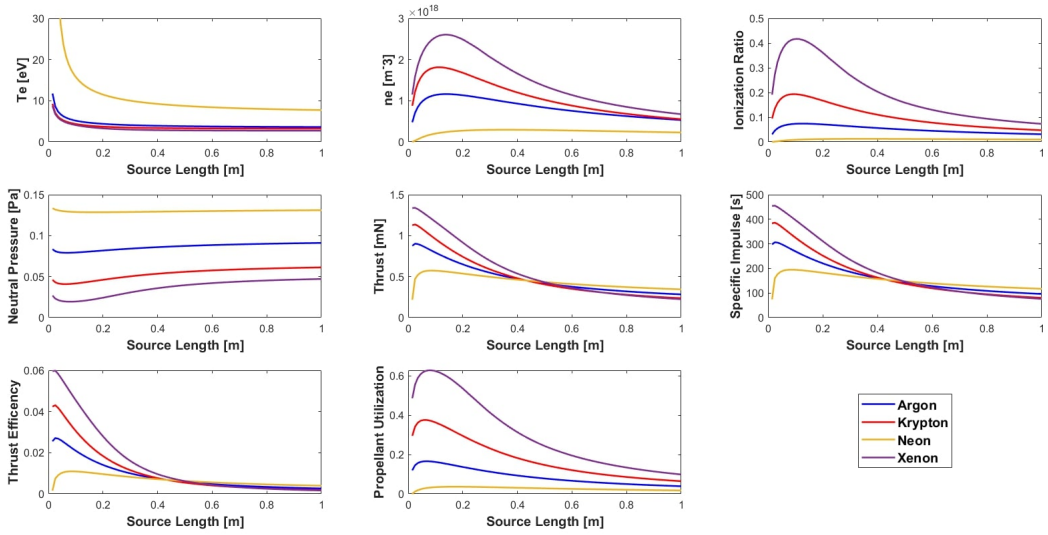

Figure 2.15: *Output parameters in function of source length*

figure 2.15 we can conclude that:

- The characteristics of the plasma are represented by curves which in some sections are quite distinct from each other. The same curves suggest that there is an optimal source length value to maximize the electron density n_e and the ionization ratio, but not T_e and n_e.

- By carefully observing the curves that describe the propulsive performance, we notice that most of them have a maximum even if for thrust, specific impulse and thrust efficiency it is difficult to recognize: a more detailed analysis showed clearly that for low values of source length there exist a maximum over the The

intersection between the curves that is present in the thrust, specific impulse and thrust efficiency graphs suggests that there is a certain length of the source such that a different choice of propellant gas would not bring any benefit for these quantities.

2.4 Propellant gas choice

Before proceeding with the choice of propellant gas, there is an important question to be asked: *what are the desired requirements for the values of each parameter represented in the figures above?*

We can break down the desired requirements as follows:

- **High value requirement**

  $$n_e$$

  Ionization ratio

  Thrust

  Isp

  $$\eta$$

  If the values of these parameters are high, an optimal plasma density in the source is guaranteed together with the best propulsive performances.

- **Low value requirement**

  $$T_e$$

  Neutral pressure

  If these parameters are characterized by reduced values, a high plasma density in the source and a good stability of the plasma itself are guaranteed, which would instead become unstable if the temperatures were too high.

Proceed with the choice of the propellant gas by referring to the graphical results described in the previous section. Note how in figure 2.12 and in figure 2.14 (relative to *Magnetic field intensity* and *R*) Xenon always guarantees better propulsive performance than all other gases. To correctly evaluate the graphs that describe the other parameters as the mass flow rate, the electrical power and the length of the source vary, it is good to make further clarifications.

1. **Mass flow rate**

   To define which gas guarantees the best propulsive performance, it is useful to have an estimate of the mass flow values that will flow into our engine. From figure 2.11 we note that while the value of *Isp* grows exponentially as the mass flow rate decreases, the graphs of *Thrust*, η and *Propellant utilization efficiency* show maximums for mass flow values between $\left[0.3 \times 10^{-9} kg/s, 1 \times 10^{-9} kg/s\right]$. Within this range in particular, Xenon stands out as the best propellant.

2. **Electrical power**

   The electric power available on board is strongly limited by the dimensions of solar panels mounted on the hosting satellite. We know that for these satellites the standard of power supplied to the propulsion block is $\sim 50W$ [4]. In the range $[0.5W, 50W]$ the Xenon again has the most desirable characteristics.

3. **Source length**

   Again, the standard size of a CubeSat unit is $0.1m$ and defines the upper limit of source length. From figure 2.15 it is clear that in the possible range of values $[0.01m, 0.1m]$ it is Xenon that guarantees the best performance.

We can undoubtedly conclude that on the basis of the simulations we performed, Xenon is the best gas to use as a propellant on REGULUS. From now on, the optimization of our Helicon Plasma Thruster will proceed with one less variable, since the propellant gas to use is no longer an unknown in our problem.

2.5 HPT optimization

Now that the propellant gas has been chosen, the methods for optimizing the other five input parameters remain to be defined. We remind the five remaining input parameters to be: mass flow rate, magnetic field intensity, electrical power, source radius and source length. However, we can refer to the graphs presented in the previous section to try to have the clearest possible view. Before delving into the resolution of this problem, it is necessary to find an answer to this fundamental question: *which propulsion parameter is this optimization interested in maximizing?*

The answer to this question is by no means obvious, since for different mission profiles there may be different requirements to satisfy: if, for example, REGULUS was required for an interplanetary mission, Δv would be by far the most relevant parameter, while for an engine that were to perform orbit changes or station keeping would be the Thrust to become the fundamental requirement [21]. Since this thesis work is not aimed at optimizing a thruster for a given mission, thrust efficiency η has been chosen as the propulsive figure of merit to be maximized. The thrust efficiency is defined in the code block describing the "propulsion_model" function.

Equation 1.22 indicates that maximizing thrust efficiency means making sure that the ratio between the kinetic power of the jet leaving the engine and the electrical power supplied is as high as possible. Following a more careful analysis of the graphs in section 2.3, further simplifications can be immediately made. It has already been noted that the curves relating to the propulsive parameters as a function of the variations of Pw and the *Magnetic Field Intensity* are monotonically increasing, and don't present any relevant maxima. In other words, all the propulsive parameters are improved the higher the magnetic field intensity and the higher the electrical power supplied. All we must do is imposing the highest possible values of these two parameters which, as we have already

explained, are $Pw = 40W$ (see equation 2.5) and *Magnetic field intensity* $= 600 \times 10^{-4}T$. Given this consideration, the parameters to be optimized remain $\dot{m}$, R and L.

2.5.1 *Thrust efficiency* in function of $\dot{m}$, R and L

If in the previous section the graphs of an output variable as a function of another input variable were drawn, this time we study the merit parameter η as a function of three input variables R, L and $\dot{m}$ (see following equation).

$$\eta = f(R, L, \dot{m}) \tag{2.6}$$

Conducting analysis with iterative cycles on all three input parameters would involve a high processing time by the Matlab software. To create the graphs of the previous section, 100 iterations were performed for each parameter (defined in line 49 in figure **??**). If vectors were constructed with 100 elements for each of the three input parameters to the function in equation 2.6, the number of iterations to be performed would be 100^3 or 1000000 iterations. Considering an average time for each of them of about $20s$, it would take about 231 days to obtain a first solution. Nor should we overlook the fact that such a solution would present a very high level of uncertainty. Let us take for example the length of the source, which in the previous analyses was studied along an interval of extremes $[0.01m,\ 1m]$: if this interval were divided into 100 parts, one would obtain an uncertainty of $\pm 0.0099m$, clearly too high for a thruster up to $0.1m$ long. These issues are resolved by adopting the following methods:

1. *Mass flow rate outside of iterative cycles*

   Instead of setting iterative cycles on three variables, the mass flow rate is imposed on line 2.11 before launching the simulation and iterative cycles are performed only on the geometry of the source, therefore on R and L. In this way it is possible to obtain graphical results that are easily interpretable and are displayed on the screen in two ways: one uses the "surf" function while the other uses the "contourf" function of Matlab.

   "Contourf" works in a similar way but is represented only in 2D as the X and Y coordinates always represent L and R, while the thrust efficiency is represented on the graph by different shades of colors, while the values of η are presented to the reader with the aid of contour lines (figure 2.16a).

   "Surf" defines a set of points in space where the X coordinate represents the radius of the source (R), the Y coordinate represents the length of the source (L) and the Z coordinate indicates the thrust efficiency η related to each combination of R and L considered (figure 2.16b).

   The mass flow values that are set manually for every possible case are the elements of the vector in equation 2.7:

   $$\dot{m} = [50, 70, 90, 110, 130, 150, 170, 190, 210, 230, 250, 270, 290, 300]\, e^{-9} kg/s \tag{2.7}$$

2. Vectors of L and R of up to 10 elements

   Having only two iterative cycles to do, the number of iterations is imposed as a maximum of 10^2, that means 100 iterations for each mass flow value expressed in the equation 2.7.

3. Extrema of the vectors of L and R around the known maxima

   In section 2.3 a preliminary analysis of the propulsive performance as the geometry varies has already been conducted. To ensure that the intervals between the extremes of the vectors are smaller than in section 2.3 , we choose to study the values of R and L in a neighbourhood of the optimal values identified in figures 2.14 and 2.15. The breadth of this neighborhood is defined arbitrarily from time to time, seeking a compromise between the limits already described and the interest of having a vision on a spectrum of values that we want as wide as possible.

We see in the figures below an example of the graphs obtained. The label of the figures indicates the mass flow rate to which they refer.

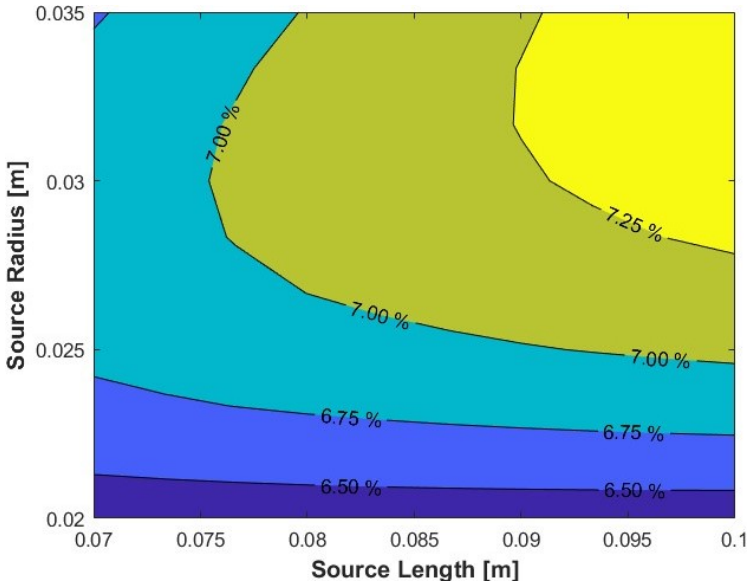

(a)

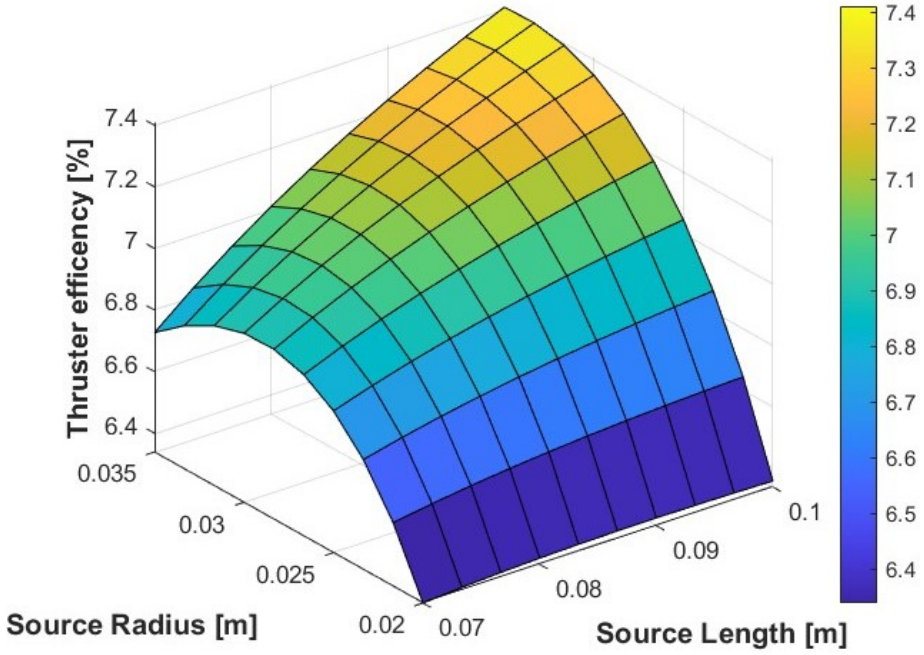

(b)

Figure 2.16: (a) *Contourf graph for* $\dot{m} = 110e - 9kg/s$ (b) *Surf graph for* $\dot{m} = 110e - 9kg/s$

Based on the graphs shown in figure 2.16a and 2.16b, it is advisable to make the following clarifications:

- The graph of the "contourf" function is set to show contour values only for η values included in the interval $[4, 7.5]$ %.
- The graph of the surf function indicates that there is an optimal source radius, but

not an optimal source length for maximizing η. A surface that would be dome-shaped could have been expected, but for the mass flow rate under consideration this is not the case. Clearly, the length of the source that would maximize the thrust efficiency would be larger than the side of the CubeSat.

- It has already been mentioned that the extrema of the vectors of L and R are chosen arbitrarily for each different value of $\dot{m}$. For the choice of these values, two criteria are mainly followed: The first takes into consideration the dimensions of the CubeSat and, considering that maximum R is $0.03m$ and maximum L is $0.1m$, the thrust efficiency is studied around these two values. The second criterion, on the other hand, is necessary because the differential equations solved during the iterations do not always find a convergent solution for all combinations of R and L. In these cases, it is plausible that the interval between the extremes is too large and should be reduced, so that it is always possible to obtain a solution that is convergent. This latter issue is particularly relevant for lower mass flow values, where two things may happen: either the T_e is too high to guarantee stability to the solution or the volume is too large for a small amount of gas, preventing the achievement of the plasma density necessary to ensure the right stability over time. Since these problems mainly concern the extrema of the vectors of R and L considered, it will first be necessary to perform a solution cycle of 4 iterations, one for each combination between the extrema of the vectors R and L. If the Matlab code can provide a solution for all the combinations of the four extremes, it is very probable that it will also be able to solve all the combinations of intermediate values of L and R.

The graphs obtained for each mass flow value considered are shown in Appendix A.

2.5.2 Determination of maximum thrust efficiency

To determine the maximum thrust efficiency, it is necessary to export and archive all the data relating to the L and R iterations which are represented by figures 2.16a and 2.16b. A folder will be created for each mass flow rate considered, within which there will be three text documents, one containing the array of the considered Ls, one containing the Rs and the third a matrix describing the thrust efficiency obtained for each combination of R and L. Before defining the geometry that determines the best thrust efficiency for a given mass flow, it is good to discard data that do not meet the desired requirements. Three different requirements can be defined that distinguish valid data from invalid data, which are the followings:

1. $L \leq 0.1m$

   If the maximum η were determined by a source length greater than the dimensions of the CubeSat, this datum would be discarded in favour of another datum that satisfies this requirement.

2. $R \leq 0.03m$

   The same reasoning applies to the radius of the source, we want it to be lower than a certain limit imposed by the dimensions of the CubeSat.

3. $T_e < 15eV$

   Using Xenon as a propellant gas, for high electron temperatures, there is instability in the solution of the differential equation; this problem had already been encountered also in some of the previous simulations. It is chosen to impose an upper limit of $15eV$ of temperature to guarantee that the result is reliable and that it is the result of a convergent solution: therefore, all the combinations of L and R which determine a temperature $T_e \geq 15eV$ will be considered as invalid data.

To have a graphical comparison of these limits, see in figure the difference between the graphs obtained from the iterations (figure 2.17a) on L and R and after excluding the data that do not satisfy the requirements (figure 2.17b).

As can be seen from figure 2.17b, η values that do not satisfy the requirements are set as equal to 0: in this way, when searching for the maximum η value, these values equal to 0 will be automatically excluded. At this point it will be sufficient to write another piece of Matlab code which determines which point of the graphs in figure 2.17b is the one with the highest η, and to which values of L and R it corresponds. We then proceed by exporting the data into a vector, composed as follows:

$$vec_i = \left[\dot{m}, \eta_{max}, R_{\eta_{max}}, L_{\eta_{max}}\right] \tag{2.8}$$

Where the i index describes the $i-th$ element of mass flow vector in equation 2.7. The mass flow rate is set manually from time to time as seen in figure 2.11, while the other three elements of the vector in equation 2.8 are the result of the optimization analyses just described. The vectors are all saved in a dedicated folder, and then imported into another Matlab document to continue with the data analysis. We proceed by plotting the graphs of η_{max} as a function of $\dot{m}$, $R_{\eta_{max}}$ as a function of $\dot{m}$ and $L_{\eta_{max}}$ as a function of $\dot{m}$, represented in figure 2.18. As expected, these graphs are characterized by very rough curves, which do not allow to analyze the data as precisely as we would like. However, it is possible to define a certain trend for all the different curves:

1. **Maximum thrust efficiency curve**

   The function $\eta_{max}(\dot{m})$ has a peak in the range $[70,\ 150] * 10^{-9} kg/s$. This area of the function will later be refined to obtain the most precise final values which will lead to engine optimization. In the absence of more precise data, we can make a prediction that the maximum thrust efficiency η_{max} is reached for a value of $\dot{m}$ around $100 * 10^{-9} kg/s$.

2. **Optimal source radius curve**

   Note that the source radius increases rapidly as the mass flow rate injected into the source increases, until it reaches the maximum value of $0.03m$ which is imposed

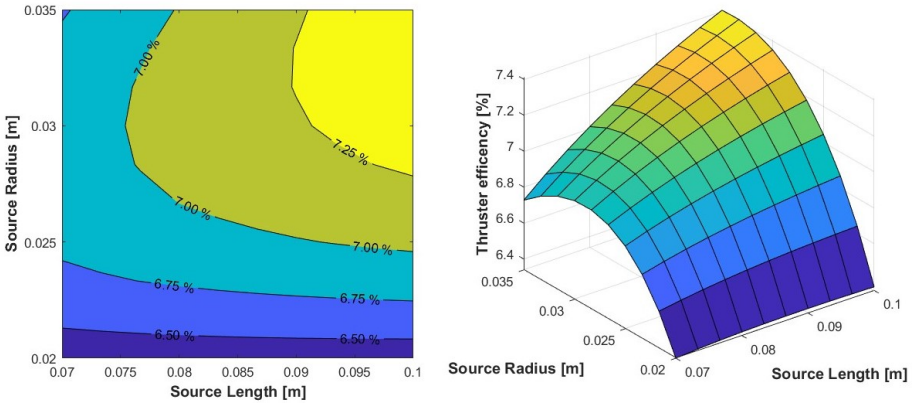

(a)

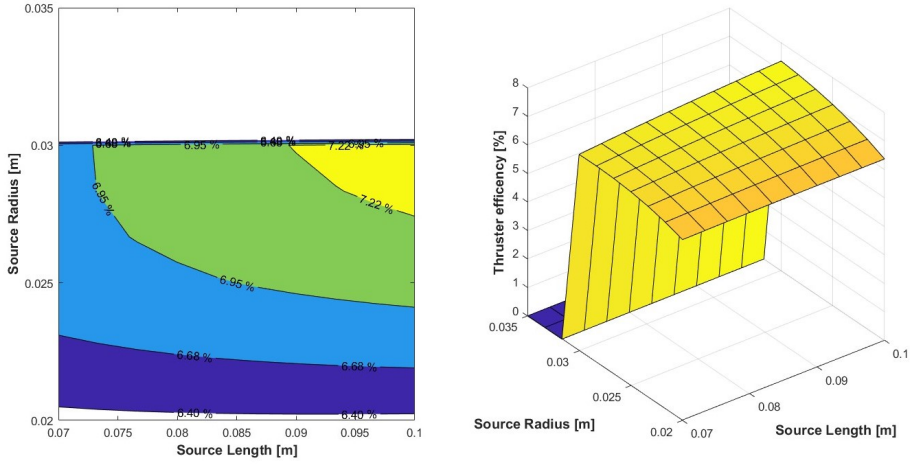

(b)

Figure 2.17: (a) *Contourf and Surf graph for $\dot{m} = 110e - 9kg/s$, before data selection* (b) *Contourf and Surf graph for $\dot{m} = 110e - 9kg/s$, after data selection*

by the limits already discussed in this section. It is also clear, despite the high uncertainties, that the radius of the source that maximizes η will be around the set limit. We will try to validate this hypothesis through subsequent more precise analyses.

3. **Optimal source length curve**

   As happens for the optimal source radius curve, the source length curve also grows rapidly as the mass flow rate increases and then reaches the limit of 0.1m set in this section. Beyond the mass flow rate value of $1.5 \times 10^{-9} kg/s$ the curve seems to take on a decreasing monotonous attitude, but this impression must not overlook the high uncertainties relating to these data.

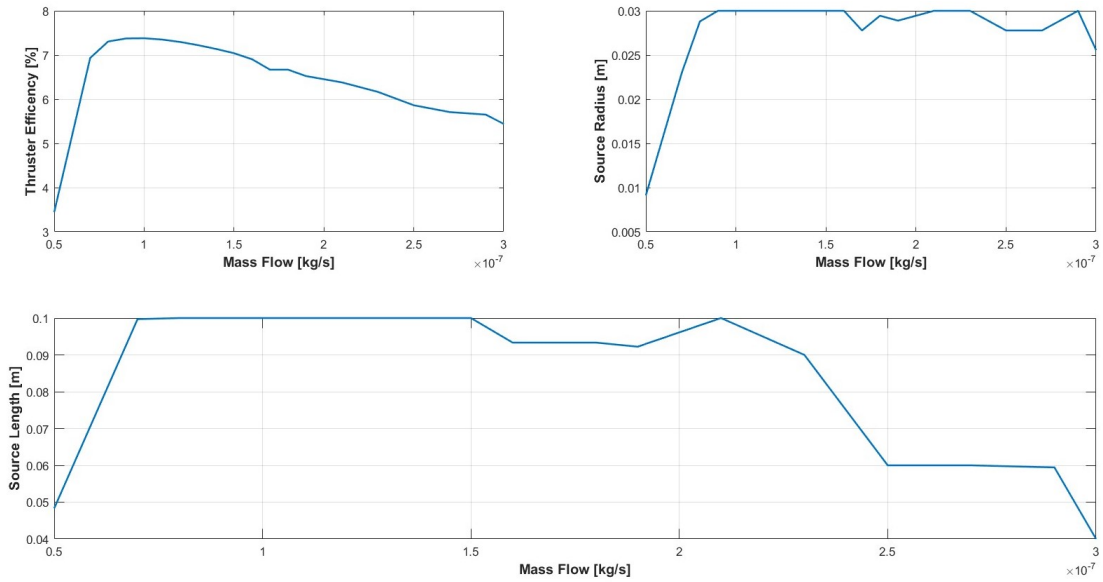

Figure 2.18: η_{max},$R_{\eta_{max}}$,$L_{\eta_{max}}$ *in function of* $\dot{m}$

–3–
Data analysis with uncertainity requirements

Once these first results have been obtained, we proceed with the analysis until we obtain data with levels of uncertainty that are lower than a certain value. The question that arises now is: *how do you define an uncertainty value that is low enough?* The answer lies in the nature of the same quantities that we want to optimize:

1. **Uncertainty about $\dot{m}$**

   In the T4i laboratory we know that, for technologies similar to REGULUS, it was possible to control a Xenon mass flow rate with a sensitivity of $2{\times}10^{-9} kg/s$. Based on this last datum, it was decided to adopt $\pm 2 \times 10^{-9} kg/s$ as the maximum uncertainty on the $\dot{m}$ values.

2. **Uncertainty about L and R**

   The geometric parameters of the size of the source will instead depend on the technologies used for the machining. From the data provided by the T4i laboratory, we know that the machining comes to model the components with an accuracy of a tenth of a millimetre. This is the value of $\pm 1 \times 10^{-4} m$ that we have chosen to adopt as the maximum permissible uncertainty on the geometric measurements of the source.

Before proceeding with the subsequent analyses, we must reflect on the computational cost of these new precision requirements. Assume, absurdly, that we have to conduct this analysis with the preliminary vectors defined in section 2.3, which had extremes of $[45, 300] \times 10^{-9} kg/s$ for the vector of $\dot{m}$, $[0.002, 0.12]\, m$ for the vector of R and $[0.015, 1]\, m$ for the vector of L. To satisfy the precision requirements, the vectors of the three quantities should have a number of elements which is equal to:

$$number_{elements} = \frac{extreme_{superior} - extreme_{inferior}}{uncertainity} \tag{3.1}$$

From equation 3.1 it results that the vector of $\dot{m}$ will have a number of elements equal to 127, the vector of R will have a number of elements equal to 1180 while the vector of L will have 9850 elements. Multiplying together the number of elements of the three vectors, we get the total number of iterations to perform, which is about 1.5 billion iterations. It is therefore clear that to proceed with this calculation it is first necessary to adopt suitable simplification strategies.

3.1 Simplification of geometry iterations

From the graphs in figure 2.16a and 2.16b we can see how the "Contourf" and "Surf" functions determine the point that represents η_{max}, $R_{\eta_{max}}$ and $L_{\eta_{max}}$ for a given flow rate massive. To increase the precision of the analysis we have chosen to perform these iterations again, but this time with a new definition of the extrema of the vectors of R and L. Once the optimal value of R and L which maximizes the thrust efficiency has been determined, the new extrema of the vectors of R and L for the subsequent analyzes are defined as follows: the element preceding the optimal value will become the lower extremum, while the element following the optimal value will become the upper extremum. In figures 3.1a and 3.1b we have a graphical representation of this procedure, where the red dot indicates the combination of R and L which determines η_{max}, while the green dots represent the new extremes of the vectors used for the subsequent analyses. See a numerical example to better understand this procedure, relating to the mass flow rate of $\dot{m} = 170e-9kg/s$. The initial vectors chosen for the preliminary analysis are:

$$\begin{aligned} L &= [0.04,\ 0.0489,\ 0.0578,\ 0.067,\ 0.075\ , 0.084,\ 0.093,\ 0.102,\ 0.111,\ 0.12]\, m \\ R &= [0.02, 0.0239, 0.0278, 0.03167, 0.0356, 0.0394, 0.0433, 0.0472, 0.0511, 0.055]\, m \end{aligned} \tag{3.2}$$

The maximum thrust efficiency $\eta_{max} = 6.67\%$ is determined by the combination of the two optimal dimensions:

$$\begin{aligned} L_{\eta_{max}} &= 0.093m \\ R_{\eta_{max}} &= 0.0278m \end{aligned} \tag{3.3}$$

According to vector L in figure 3.1, the element before the optimal value is $0.084m$ and the element after it is $0.102m$. For the vector of R in figure 3.1, the element before the optimal value is $0.0239m$ and the element after it is $0.03167m$. The new vectors for subsequent analyses will be defined by the "linspace" function, as written below:

$$\begin{aligned} L_1 &= linspace\left(0.084m, 0.102m, n_{iter_L}\right) \\ R_1 &= linspace\left(0.0239m, 0.03167m, n_{iter_R}\right) \end{aligned} \tag{3.4}$$

Where usually $n_{iter_L} = n_{iter_R} = 10$ This analysis will provide two new values of $R_{\eta_{max}}$ and $L_{\eta_{max}}$, and this procedure is repeated until the underlying condition, deriving from equation 3.1, is satisfied:

$$uncertainity >= \frac{extreme_{superior} - extreme_{inferior}}{n_{iter}} \tag{3.5}$$

It is probable that one of the two dimensions will satisfy this condition before the other; it will be sufficient to decrease the number of iterations for the first quantity and increase the number of iterations for the quantity which has not yet satisfied condition in equation 3.5.

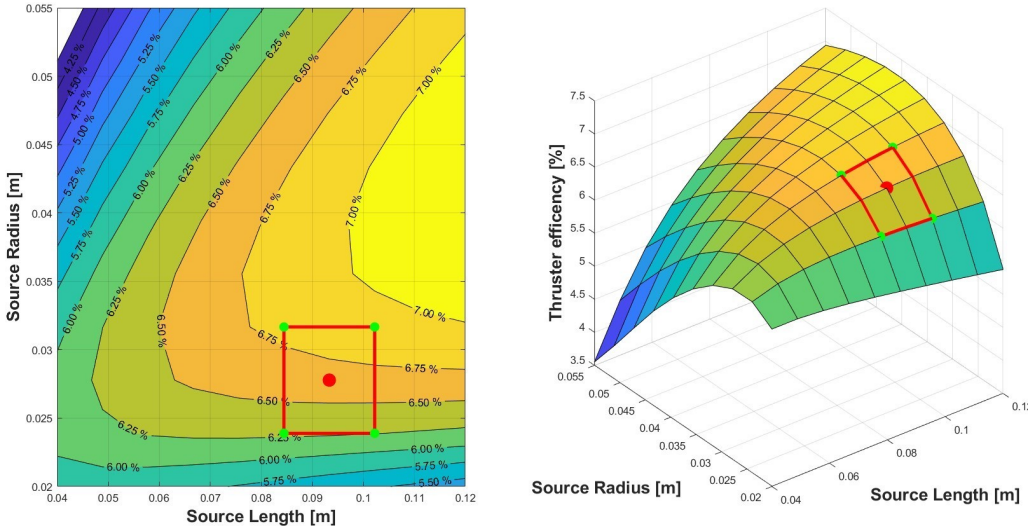

(a)

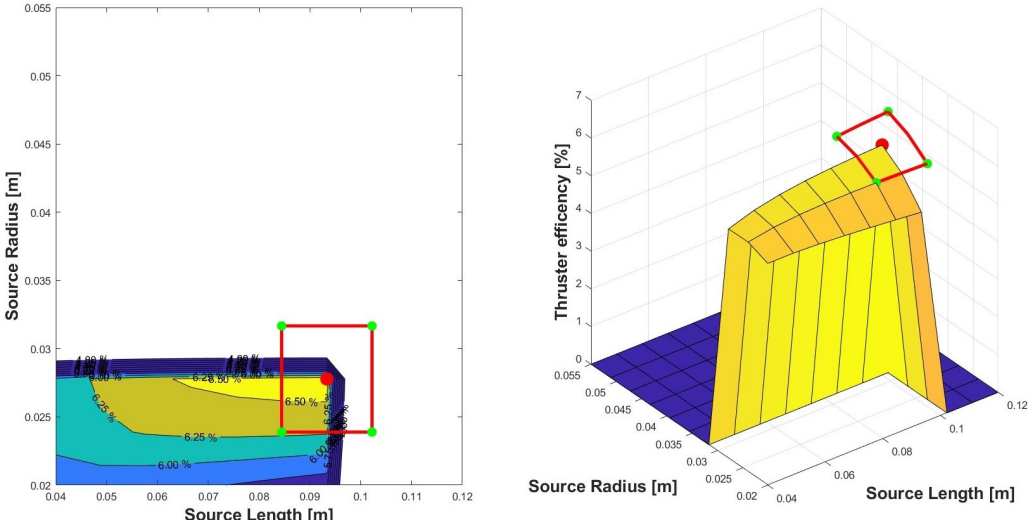

(b)

Figure 3.1: (a) *Contourf and Surf graph for* $\dot{m} = 170 \times 10^{-9} kg/s$*, before data selection, with representation of next iterations' domain* (b) *Contourf and Surf graph for* $\dot{m} = 170 \times 10^{-9} kg/s$*, after data selection, with representation of next iterations' domain*

3.2 Simplification of Mass Flow Iterations

Observing the graph in figure 2.18 relative to η_{max} as a function of $\dot{m}$, it was possible to distinguish a certain trend despite the high uncertainty: it has already been hypothesized that the peak of η_{max} is determined for mass flow values included in the interval $[0.7,\ 1.5]\times 10^{-9}kg/s$. To arrive at precise results on the value of $\dot{m}$ that maximize η_{max}, it will be sufficient to carry out the analyses only in this last range of mass flows. The difference between one mass flow rate value and the previous one must be taken into consideration, making sure that the value of this difference is less than or equal to the sensitivity with which the mass flow rate is controlled, which is $2 \times 10^{-9}kg/s$. Having made these considerations, we can define the mass flow rate values to be analysed, which are grouped in the underlying vector:

$$\begin{aligned}\dot{m} = [&70, 72, 74, 76, 78, 80, 82, 84, 86, 88, 90,\\ &92, 94, 96, 98, 100, 102, 104, 106, 108, 110,\\ &112, 114, 116, 118, 120, 122, 124, 126, 128, 130,\\ &132, 134, 136, 138, 140, 142, 144, 146, 148, 150] * 10 - 9kg/s\end{aligned} \tag{3.6}$$

Thanks to these simplifications, the number of iterations will be significantly reduced. For each mass flow, the vectors of L and R must be combined for a total of 100 combinations. Assume that the process is repeated on average 5 times to meet the required precision requirements, obtaining a total of 500 iterations for each mass flow value: multiplied by all the mass flow values we want to study, we obtain approximately 20000 iterations, which is clearly a smaller number than the one obtained at the beginning of this chapter.

3.3 Final results

Figure 3.2 shows the graphs resulting from the more precise analysis just described. Only the mass flow values contained in the vector in equation 3.6 are represented on the abscissas of these graphs. Given the higher precision of these data, the curves turn out to be a lot smoother and trends are much more easily analysable. As expected, the η_{max} curve has a peak in the interval considered, confirming that the trends obtained following the roughest analyses still provided reliable results. The optimal R and L curves, on the other hand, tend to quickly reach a flat trend, given that the upper limits have been imposed on these two dimensions, respectively $0.03m$ and $0.1m$. All that remains is to analyse these curves more closely to obtain a geometric configuration and a mass flow value that optimize η. From the graph in figure 3.3 we can have a more detailed view of the peak on the η_{max} curve. From the graphs in figure 3.3 it emerges that the optimal values of R, L and $\dot{m}$ can be obtained, reported in equation 3.3.

$$\begin{aligned}R_{\eta_{max}} &= (0.03 \pm 0.0001)m\\ L_{\eta_{max}} &= (0.1 \pm 0.0001)m\\ \dot{m}_{\eta_{max}} &= (96 \pm 2) \times 10^{-9}kg/s\end{aligned} \tag{3.7}$$

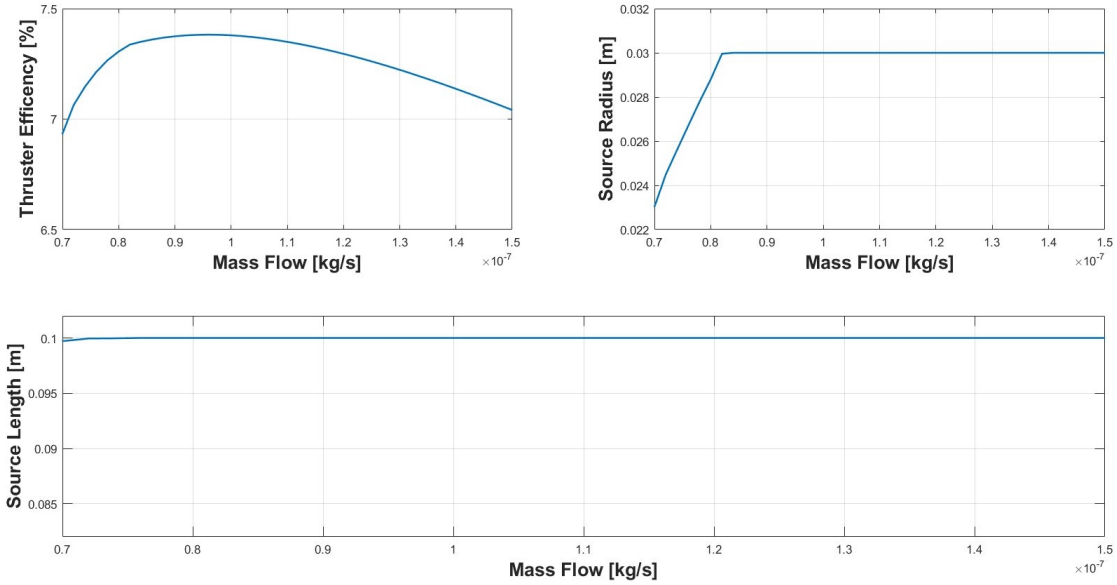

Figure 3.2: η_{max}, $R_{\eta_{max}}$ and $L_{\eta_{max}}$ curves, in function of $\dot{m}$, for $\dot{m}$ values equal to 3.6

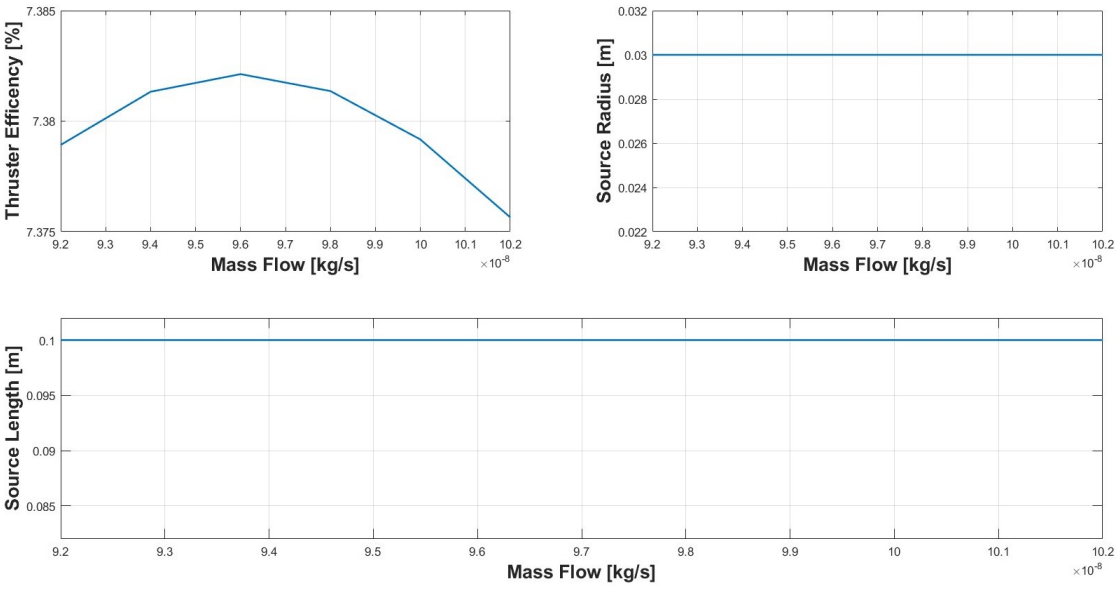

Figure 3.3: η_{max}, $R_{\eta_{max}}$ and $L_{\eta_{max}}$ curves, in detail to determine peak of η_{max} curve

These values, together with the values of $Pw = 40W$ and *Magnetic Field Intensity*= $600 \times 10^{-4}T$ define a value of η_{max} equal to:

$$\eta_{max} = (7.39 \pm 0.0007)\% \tag{3.8}$$

Plasma thrusters similar to REGULUS (in terms of size and electrical power) are characterized by thrust efficiencies of the same order of magnitude, which confirms the good quality of our analyses.

–4–
Further Analysis

We summarize in the following lines all the input values resulting from the optimization of the propulsor:

- $\dot{m} = 96 \times 10^{-9} kg/s$
- $Magnetic\ Field\ Intensity = 600 \times 10^{-4} T$
- $Pw = 40W$
- $R = 0.03m$
- $L = 0.1m$

We recall how these results were obtained through an analysis that imposed limits of both a technological and geometric nature. Faced with the values obtained, the following question arises spontaneously: *Which of the dimensional and technological limits that have been imposed is the one that has most limited the maximization of the thrust efficiency value?* An initial answer to this question could be hidden in a more careful observation of the graphs obtained following the preliminary analysis, where the trends of the propulsive parameters were studied as each parameter in input to the system varied. However, it is good to first ask ourselves whether those graphs, obtained from preliminary values deriving from a similar engine, are sufficiently representative of the engine that we have managed to optimize in this draft. To get a clear answer, let's pay attention to figure 4.1: In the graph on the left, two color lines have been integrated on the surface, which represent the trends of η as a function of L for two different constant values of source radius R (see legend in figure 4.1). In the graph on the right, the same curves are put comparison, to have a clear view of how the trend of η as a function of L is strongly influenced by the value of R that is chosen. Following these considerations, we can conclude that in order to have a precise view of how the various input parameters can influence the propulsive performance of our HPT specifically, the graphs obtained in section 2.3 will have to be drawn again, taking care to impose the chosen values as the values appearing at the beginning of this chapter. Since our optimization analysis is concerned with maximizing

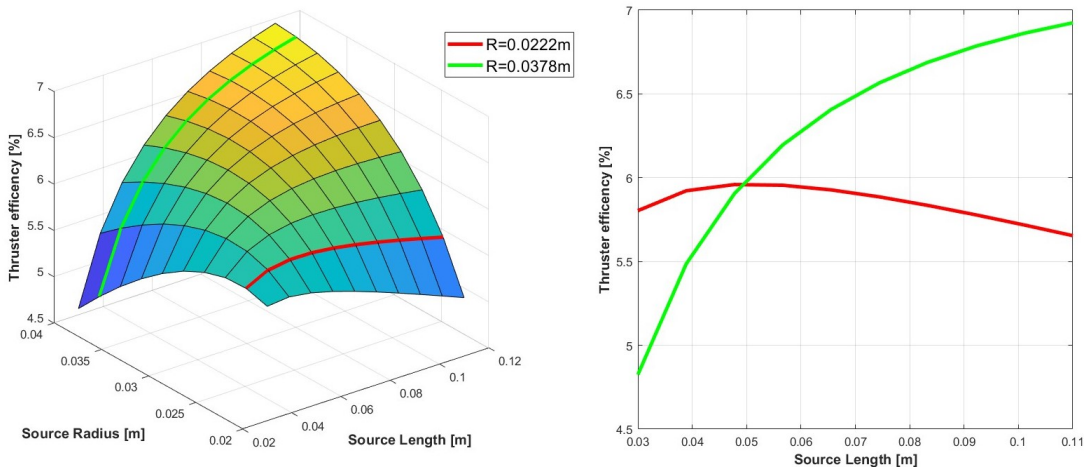

Figure 4.1: *Confront between the trend of η in function of L for two different values of R. The value of mass flow rate considered in this case is $\dot{m} = 190 \times 10^{-9} kg/s$*

η, we will then only represent the graphs relating to this specific propulsive performance as a function of all the various input parameters. The graphs relating to all the output parameters as a function of the variation of a single input parameter are collected in Appendix B.

4.1 η in function of $\dot{m}$

To evaluate how the propulsive performances vary around the optimal mass flow value, refer to figure 3.3: no limit has been imposed on the mass flow value and since it was one of the three parameters to be optimized in section 3.2, its optimal value corresponds to the maximum η value on the curve.

4.2 η in function of *Pw*

Refer to figure 4.2. On this graph it was decided to represent the results of our optimization with a green dot, while the red dot represents the maximum of the thrust efficiency curve as a function of the power output. We note how, although the electric power Pw is limited by the technology, the maximum thrust efficiency does not deviate too much from the hypothetical maximum it could reach: the value we obtain thanks to our optimization is $\eta = 7.39\%$ with a power of $40W$, while the maximum shown on this curve would be $\eta = 8.918\%$ for a power amount of $Pw = 234W$. The electrical power is known to be supplied to our thruster by the solar panels of the host satellite, which has dimensions between 6 and 24 CubeSat units. Any satellite that could supply the $234W$ of power necessary to maximize the thrust efficiency of our thruster would find itself having a very modest increase in η at the price of a major modification on the solar panels. Therefore,

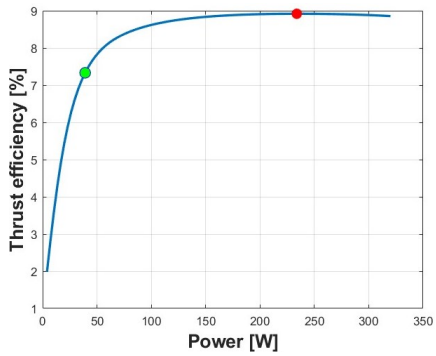

Figure 4.2: *Graphic representation of η_{max} found after precision analysis confronted with hypothetical maximum in function of Pw*

we can conclude that the optimization we performed, despite the technological limitations, represents a good engineering compromise between the two quantities.

4.3 η in function of *Magnetic field intensity*

The curve represented in figure 4.3 denotes the same behaviour as the same curve seen in section 2.3, with an increasing monotone trend without appreciable maximum points. This behaviour denotes that the higher the magnetic field, the more the thrust efficiency

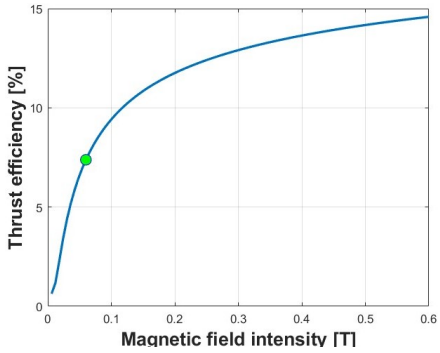

Figure 4.3: *Graphic representation of η_{max} found after precision analysis over the curve of η in function of Magnetic field intensity*

increases. We note how our optimization, also limited by technological limitations, is located on a section of the curve whose tangent line has a high slope: a possible increase in magnetic field intensity would produce significant improvements in the achievable thrust efficiency. For our optimized thruster, with a magnetic field of $600 \times 10^{-4}T$ we get $\eta = 7.38\%$. If there were a technology that allowed to generate a magnetic field of intensity $1200 \times 10^{-4}T$ occupying the same volume and with the same weight, a thrust efficiency equal to $\eta = 10.08\%$ would be obtained, a significant increase if compared with that obtained with the curve Pw. The technologies used on our engine are already

those with the most advanced state of the art, but it is good to know how a possible improvement of the same can accentuate the propulsive characteristics of our HPT.

4.4 η in function of R

From figure 4.4 it is immediately noticeable how, despite the limits imposed, the optimization of our propulsor is very close to the optimal value obtainable without imposing any limit on source radius. This fact can be interpreted in two ways:

- If our desire was to reach the maximum thrust efficiency, it would be enough to increase the radius by very little to reach the dimension that maximizes η ($R = 0.0324m$ for $\eta_{max} = 7.441\%$).
- if for some reason one wanted to reduce the radius of the source, for example to install more performing magnets, one could arrive at a radius $R = 0.0237m$ still having a thrust efficiency equal to or greater than $\eta = 7\%$. The proximity to the maximum of the curve represents an advantage in terms of dimensional tolerance of R, which can therefore be varied within certain limits without significantly affecting the thrust efficiency.

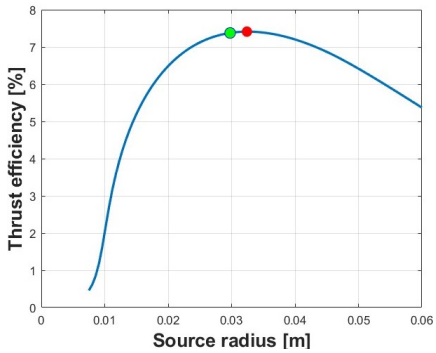

Figure 4.4: *Graphic representation of η_{max} found after precision analysis confronted with hypothetical maximum in function of R*

4.5 η in function of L

Refer to the graph in figure 4.5. Note how the optimum point determined following our analyses deviates from the maximum point of the curve $\eta(L)$ especially if compared with the proximity of the points seen with $\eta(R)$. The maximum point corresponds to a thrust efficiency equal to $\eta = 8.069\%$ as a function of a length $L = 0.3665m$: such an insignificant increase in thrust efficiency $\Delta\eta = 0.679\%$ does not justify a similar increase in source size. If we wanted to double L, we would obtain a thrust efficiency equal to $\eta = 7.946\%$,

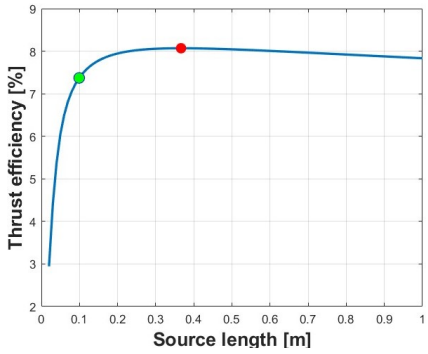

Figure 4.5: *Graphic representation of η_{max} found after precision analysis confronted with hypothetical maximum in function of L*

still too modest for such a dimensional variation. We can conclude that the limitations of L imposed by the dimensions of the CubeSat do not excessively affect the propulsive performances and any increases of the same would require too significant variations to be advantageous.

4.6 Possible improvements

Before moving on to the conclusions, a reflection was made on all those aspects of the process that could be improved in all the different analyses.

1. Matlab knowledge

   In writing the codes, solution methods based on the knowledge of Matlab acquired during studies have often been used. Such knowledge is not always sufficient to address problems inherent in plasma physics; a preliminary study is necessary for a clear understanding of the physical phenomena occurring in the source, but the current knowledge of the student does not allow a clear and rapid interpretation of the code. With a broader experience on Matlab, the student will be able to tackle the optimization problem with tools more suitable for this task.

2. Computational power

   The computational price of the Global Model is sufficiently low if one wants to perform a single simulation with static input data, but it is equally true that to face an analysis with iterative cycles the computational costs become very high, and with them the times to obtain results. To overcome these obstacles, various simplifications have been used and the work has been divided into smaller problems, gradually increasing the precision (see chapter 3). A calculator with higher computing power would be an excellent resource to use for this kind of problem, guaranteeing a precise analysis more quickly, even without resorting to simplifications of the problem.

3. Pass to next iteration in case of error

This problem was mainly encountered during the iterations in chapter 3, where R and L were combined to obtain the three-dimensional thrust efficiency graphs (see appendix A): it happened that, for some combinations of L and R at a given mass flow rate, the block of code for solving the differential equation could not reach a convergent solution, showing an error signal on the screen and interrupting the process before analyzing the successive combinations of R and L. This problem was solved by reducing the intervals between the extremes of the vectors of R and L, until all the combinations of the elements of these two vectors had not given acceptable results. However, this process inevitably leads to reducing the domain of the geometries analyzed and to neglecting some of them that could be interesting even for a preliminary study. A better idea would have been, with a better knowledge of Matlab, to force the solver block "ode_15" to skip those iterations that did not lead to a convergent solution and to continue with the subsequent ones, without necessarily having to reduce the domain of geometries to be analysed.

–5–
Conclusions

At the end of this thesis work, it is necessary to reflect on the path that has been followed.

Working on a plasma space thruster represented for the student the opportunity to study a topic that otherwise would not have been possible to explore in a normal course of study. The new knowledge that has been acquired ranges from the most varied fields, from mathematics, to programming, to plasma physics, up to scientific comunication. For the graduating student entering the world of work, the mastery of these skills represents a powerful ally to face the engineering challenges that the future holds for him.

Carrying out this work was the first approach to the modelling of complex physical phenomena such as those that occur in the presence of plasma. The Global Model implemented in the Matlab codes represented a great stumbling obstacle for the neophyte student, which he managed to overcome through meticulous study and later managed to use for his own research. The understanding and utilization of this model had to collide with the limits that this same model has hidden inside, leading the student first to identify these limits and then to define the best solutions to ensure that the model continues to operate in regimes that kept it as faithful as possible to physical reality. It has also been seen, beyond all the difficulties just mentioned, that further strategic work had to be carried out to cope with the limited computing power that a personal computer is able to offer, allowing the required results to be achieved, albeit despite the poorly performing means. The achievement of a first result, although it complies with all the required requirements, has placed the student in the position of having to question his work again, asking himself a different question each time and looking for answers that demonstrate the validity of the procedure carried out.

Of fundamental importance in this process was the help of a supervisor, someone who dedicates their time to guiding those who are approaching these topics for the first time. A path of this difficulty would not have been possible without the help of those who are able to teach; not only to transmit knowledge, but to instil in the listener the desire to learn more.

Ultimately, it is also good to mention the feeling of belonging that working on this thesis has given rise to in the student, of the collaboration with a team of other researchers to achieve a common goal, driven by the desire to see the evolving future of man into

space.

Appendix A
"*Contourf*" and "*Surf*" plots for all $\dot{m}$

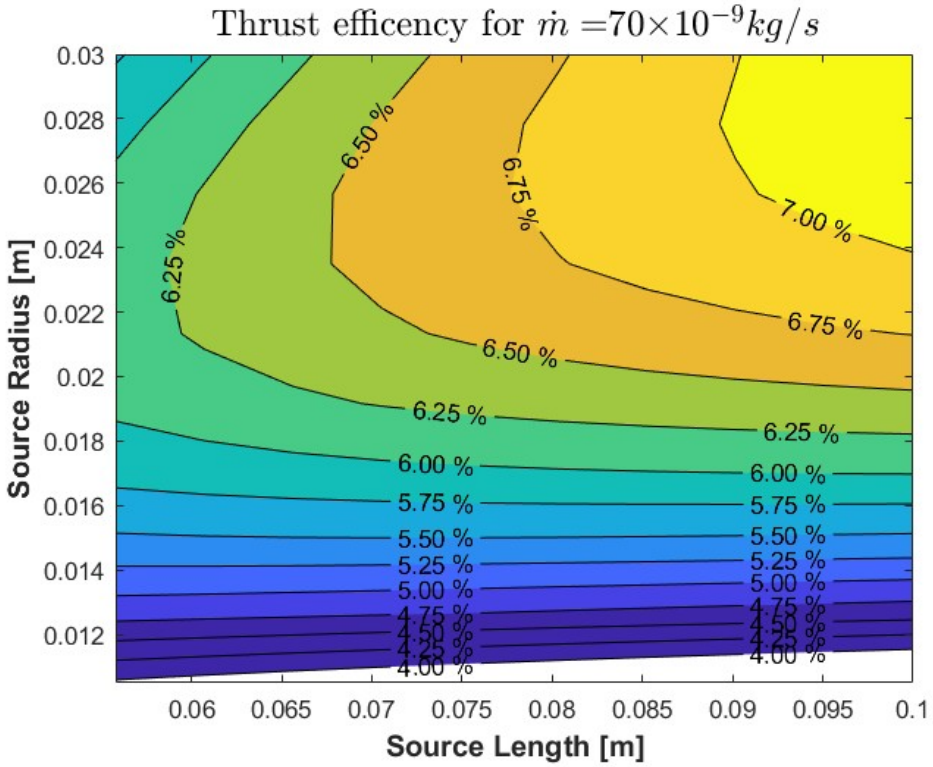
Thrust efficency for $\dot{m}$ =70×10^{-9}kg/s
Source Radius [m]
Source Length [m]
0.03
0.028
0.026
0.024
0.022
0.02
0.018
0.016
0.014
0.012
0.06
0.065
0.07
0.075
0.08
0.085
0.09
0.095
0.1
6.50 %
6.75 %
7.00 %
6.25 %
6.75 %
6.50 %
6.25 %
6.25 %
6.00 %
6.00 %
5.75 %
5.75 %
5.50 %
5.50 %
5.25 %
5.25 %
5.00 %
5.00 %
4.75 %
4.75 %
4.50 %
4.50 %
4.25 %
4.25 %
4.00 %
4.00 %

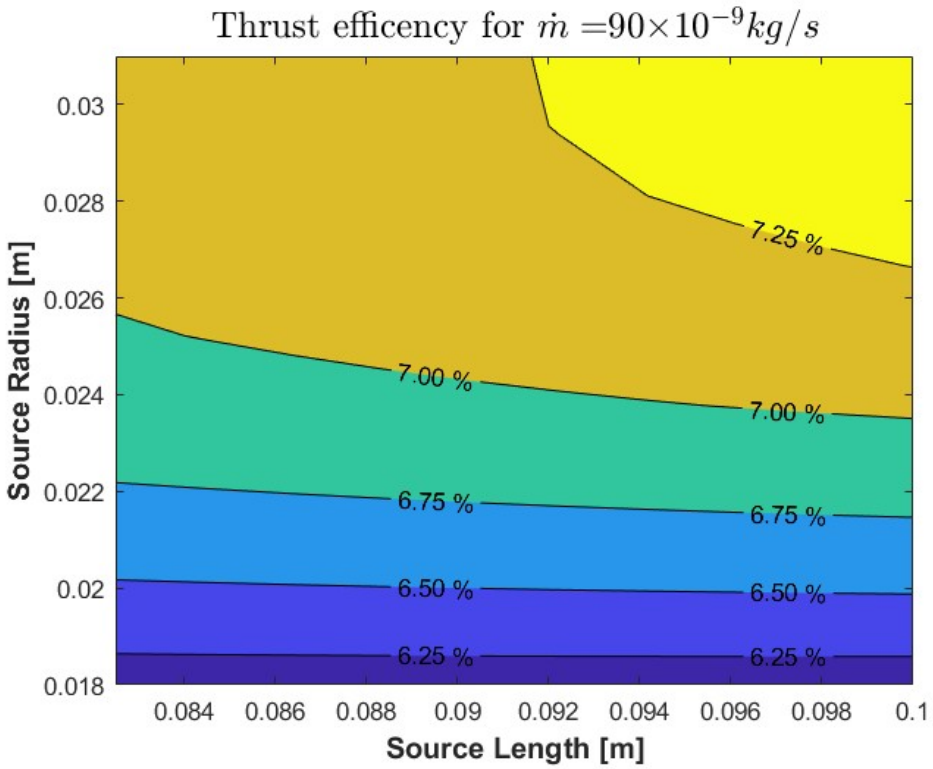
Thrust efficency for $\dot{m}$ =90×10^{-9}kg/s
Source Radius [m]
Source Length [m]
0.03
0.028
0.026
0.024
0.022
0.02
0.018
0.084
0.086
0.088
0.09
0.092
0.094
0.096
0.098
0.1
7.25 %
7.00 %
7.00 %
6.75 %
6.75 %
6.50 %
6.50 %
6.25 %
6.25 %

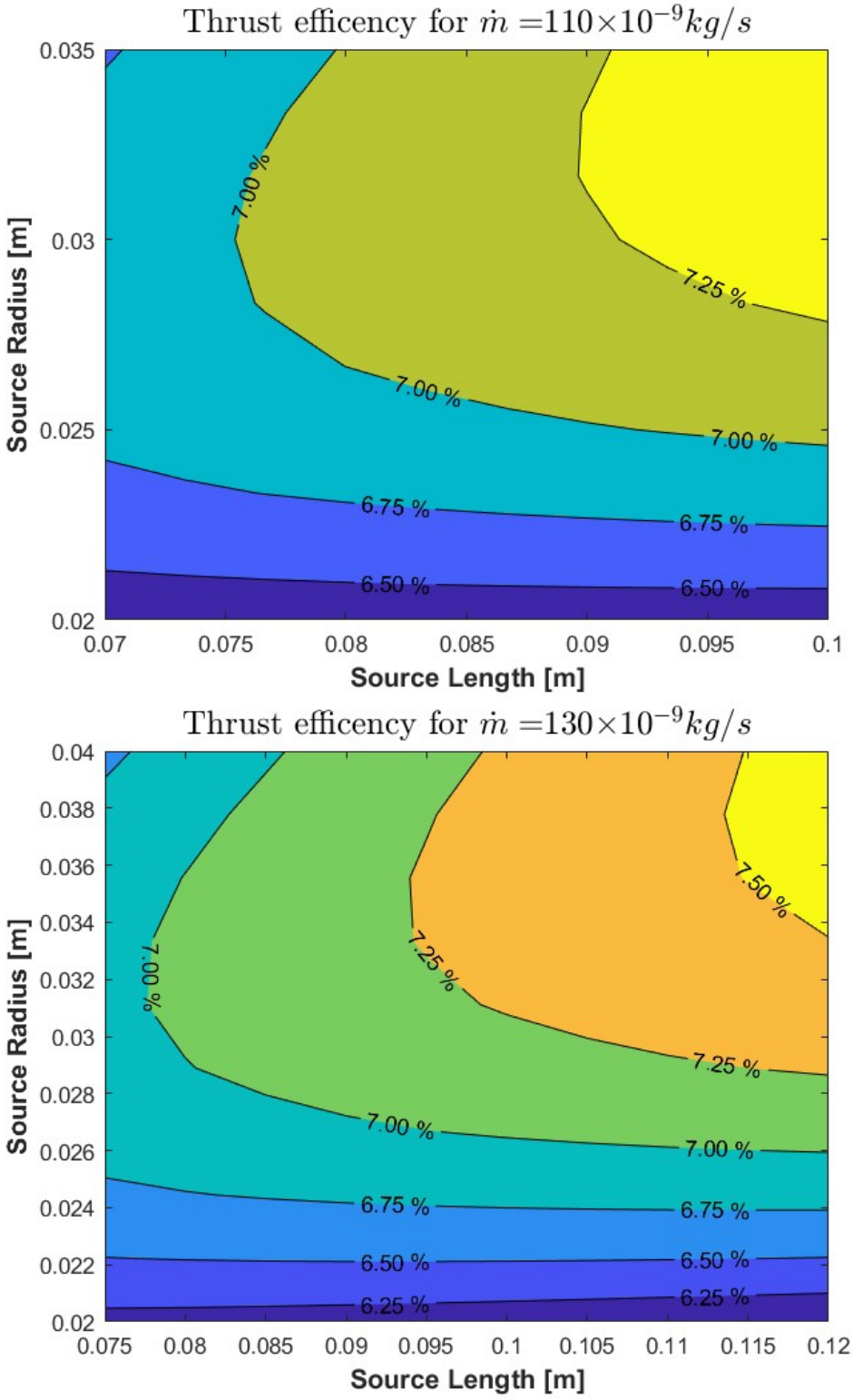
Thrust efficency for $\dot{m} = 110 \times 10^{-9} kg/s$
Source Radius [m]
0.035
0.03
0.025
0.02
0.07
0.075
0.08
0.085
0.09
0.095
0.1
Source Length [m]
7.00 %
7.25 %
7.00 %
7.00 %
6.75 %
6.75 %
6.50 %
6.50 %
Thrust efficency for $\dot{m} = 130 \times 10^{-9} kg/s$
Source Radius [m]
0.04
0.038
0.036
0.034
0.032
0.03
0.028
0.026
0.024
0.022
0.02
0.075
0.08
0.085
0.09
0.095
0.1
0.105
0.11
0.115
0.12
Source Length [m]
7.00 %
7.25 %
7.50 %
7.25 %
7.00 %
7.00 %
6.75 %
6.75 %
6.50 %
6.50 %
6.25 %
6.25 %

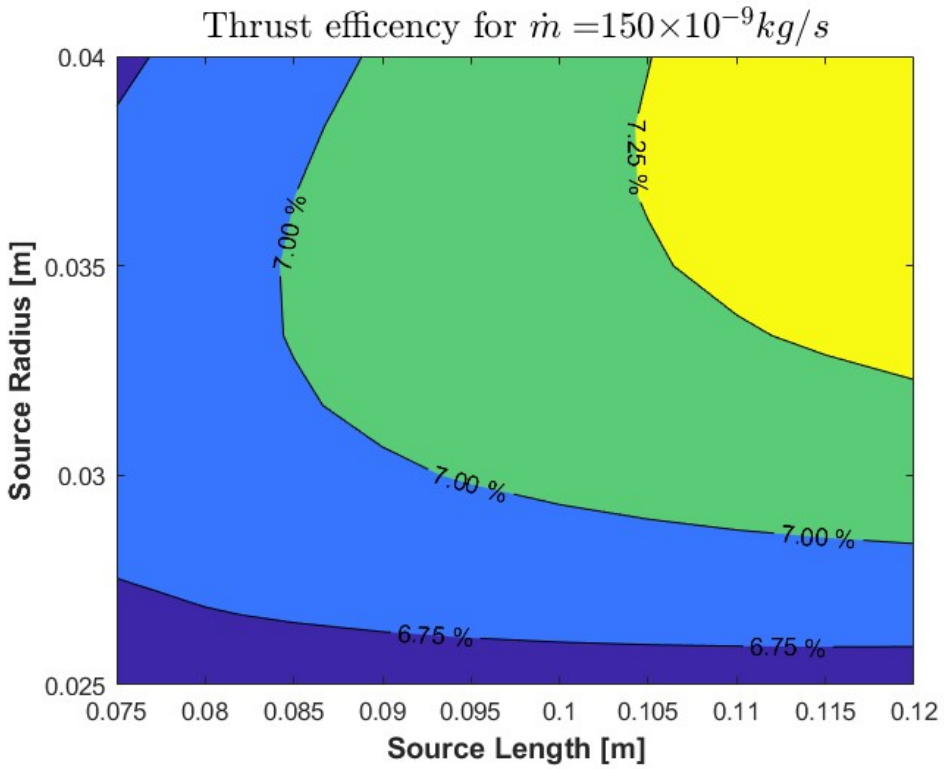
Thrust efficency for $\dot{m}$ =150×10^{-9}kg/s
Source Radius [m]
Source Length [m]
0.04
0.035
0.03
0.025
0.075
0.08
0.085
0.09
0.095
0.1
0.105
0.11
0.115
0.12
7.25 %
7.00 %
7.00 %
7.00 %
6.75 %
6.75 %

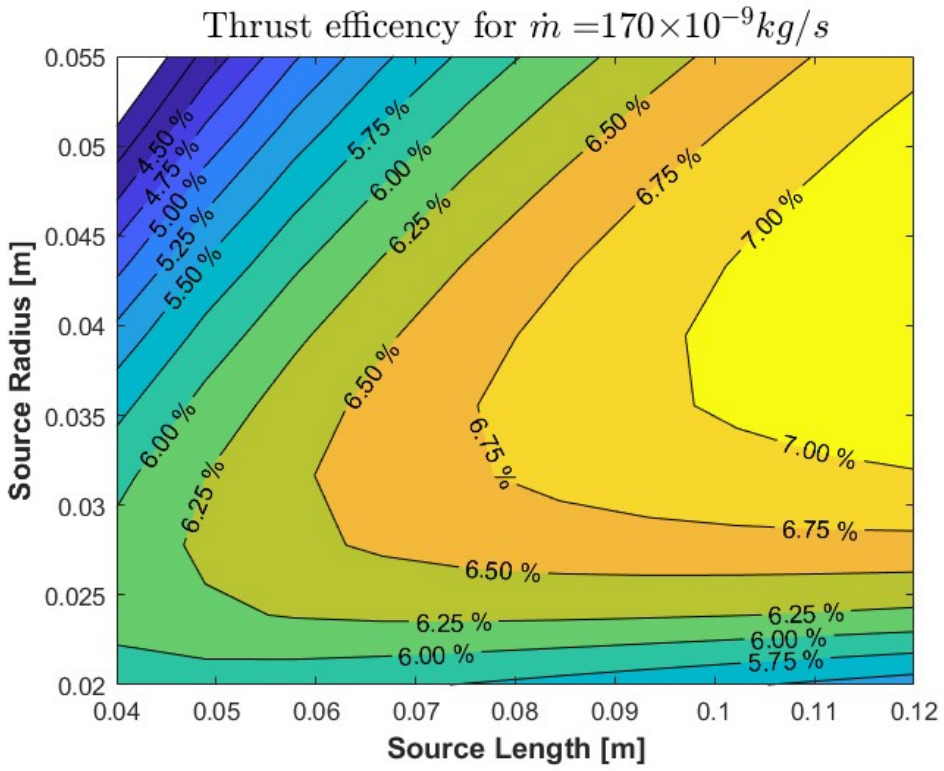
Thrust efficency for $\dot{m}$ =170×10^{-9}kg/s
Source Radius [m]
Source Length [m]
0.055
0.05
0.045
0.04
0.035
0.03
0.025
0.02
0.04
0.05
0.06
0.07
0.08
0.09
0.1
0.11
0.12
4.50 %
4.75 %
5.00 %
5.25 %
5.50 %
5.75 %
6.00 %
6.25 %
6.50 %
6.75 %
7.00 %
6.00 %
6.25 %
6.50 %
6.75 %
7.00 %
6.75 %
6.50 %
6.25 %
6.25 %
6.00 %
6.00 %
5.75 %

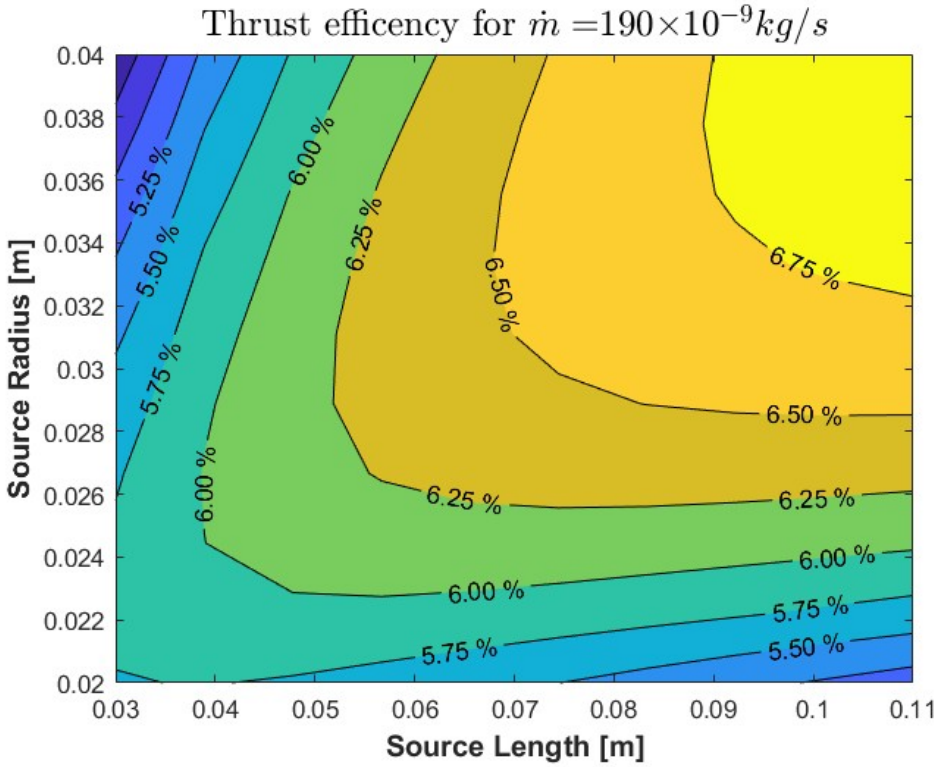
Thrust efficency for $\dot{m} = 190 \times 10^{-9} kg/s$
Source Radius [m]
Source Length [m]
0.04
0.038
0.036
0.034
0.032
0.03
0.028
0.026
0.024
0.022
0.02
0.03
0.04
0.05
0.06
0.07
0.08
0.09
0.1
0.11
5.25 %
5.50 %
5.75 %
6.00 %
6.25 %
6.50 %
6.75 %

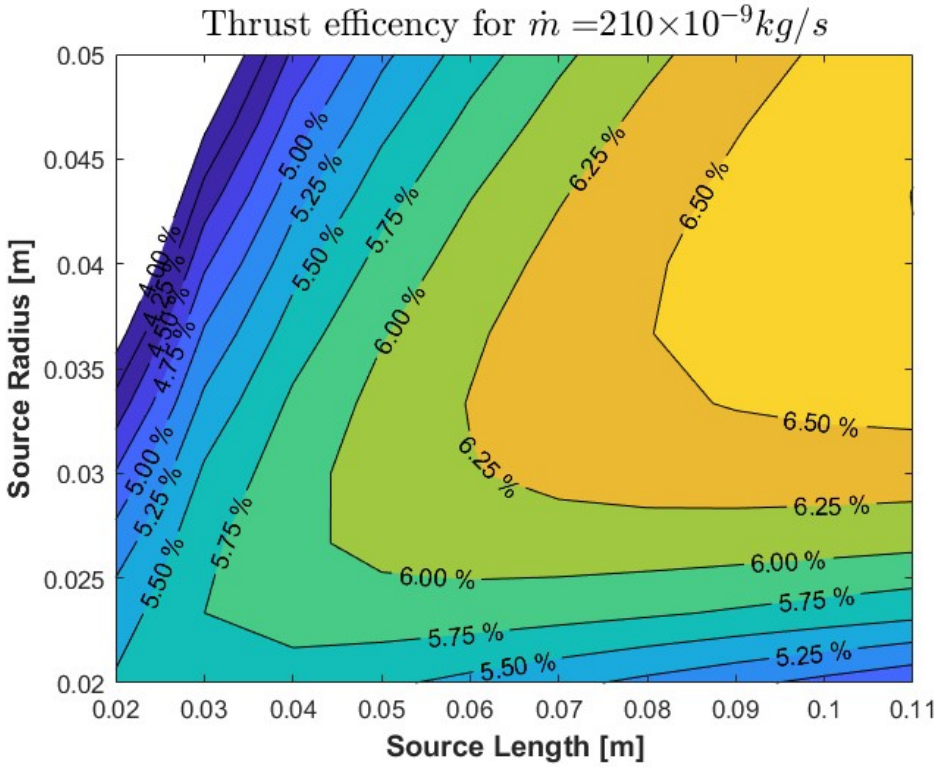
Thrust efficency for $\dot{m} = 210 \times 10^{-9} kg/s$
Source Radius [m]
Source Length [m]
0.05
0.045
0.04
0.035
0.03
0.025
0.02
0.02
0.03
0.04
0.05
0.06
0.07
0.08
0.09
0.1
0.11
4.00 %
4.25 %
4.50 %
4.75 %
5.00 %
5.25 %
5.50 %
5.75 %
6.00 %
6.25 %
6.50 %

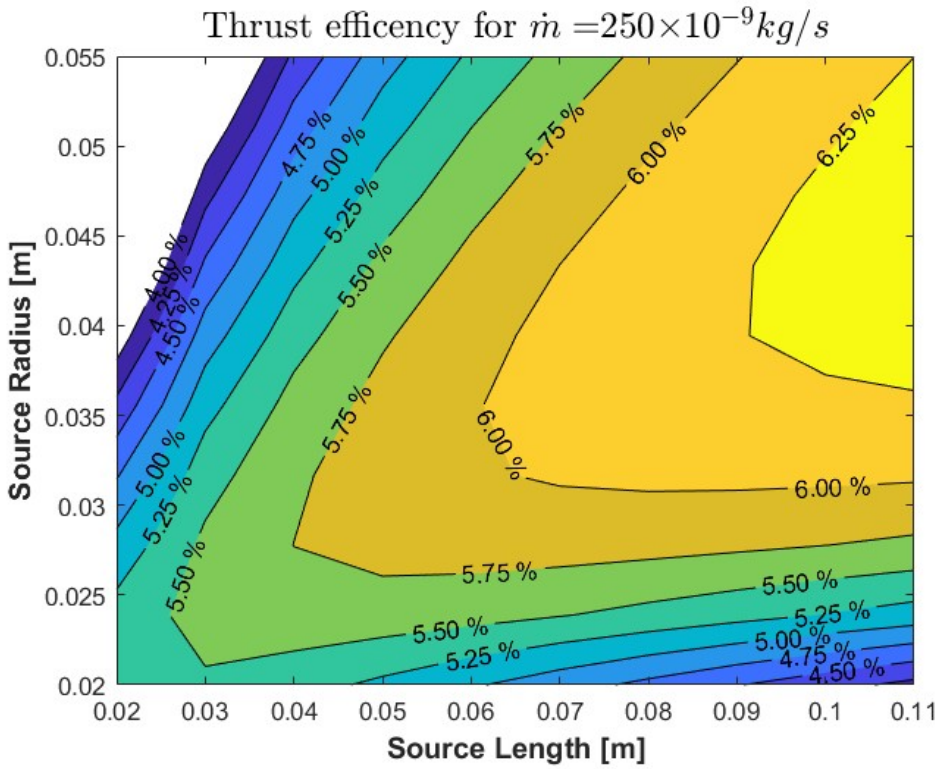
Thrust efficency for $\dot{m}$ =250×10^{-9}kg/s
Source Radius [m]
Source Length [m]
0.055
0.05
0.045
0.04
0.035
0.03
0.025
0.02
0.02 0.03 0.04 0.05 0.06 0.07 0.08 0.09 0.1 0.11
4.00 %
4.25 %
4.50 %
4.75 %
5.00 %
5.25 %
5.50 %
5.75 %
6.00 %
6.25 %

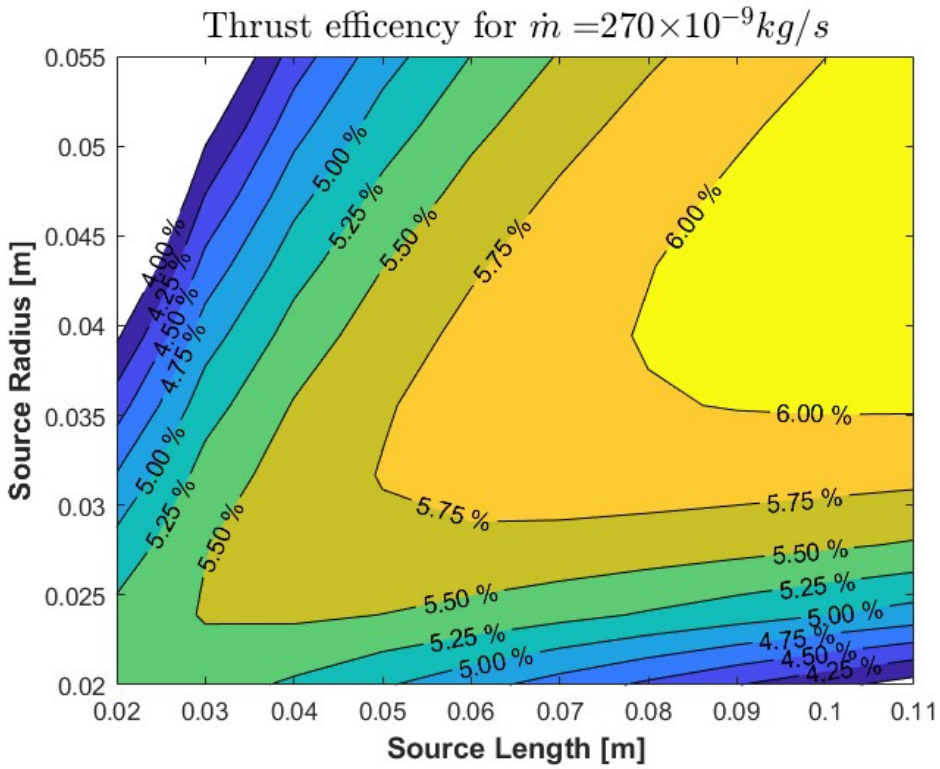
Thrust efficency for $\dot{m}$ =270×10^{-9}kg/s
Source Radius [m]
Source Length [m]
0.055
0.05
0.045
0.04
0.035
0.03
0.025
0.02
0.02 0.03 0.04 0.05 0.06 0.07 0.08 0.09 0.1 0.11
4.00 %
4.25 %
4.50 %
4.75 %
5.00 %
5.25 %
5.50 %
5.75 %
6.00 %

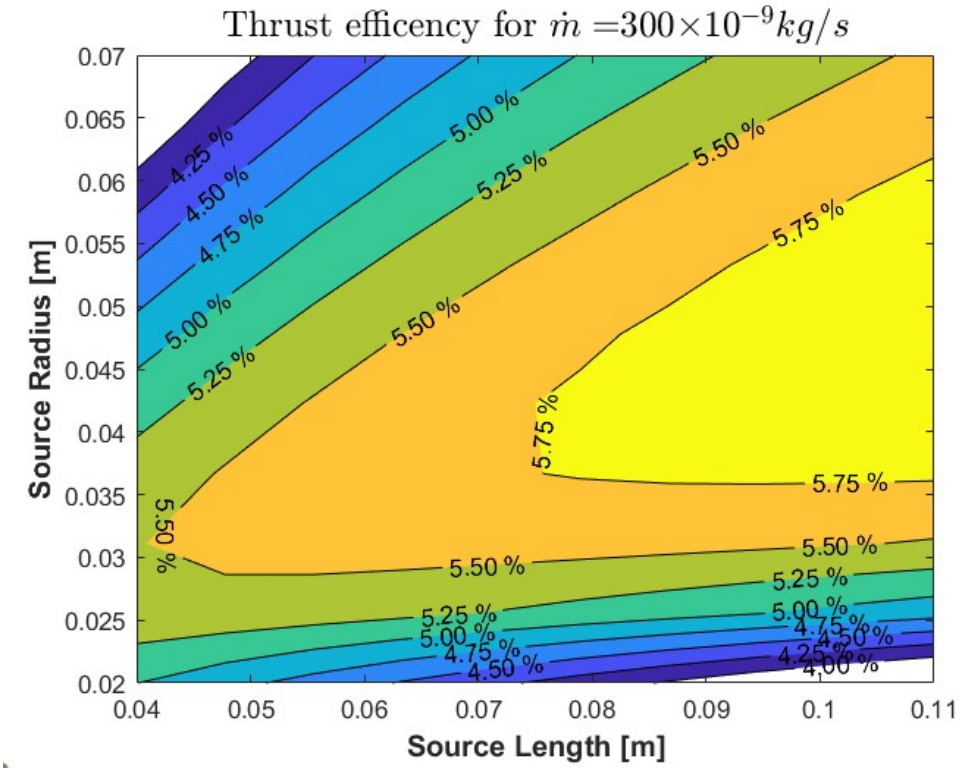
Thrust efficency for $\dot{m}$ =300×10^{-9}kg/s
Source Radius [m]
Source Length [m]
0.07
0.065
0.06
0.055
0.05
0.045
0.04
0.035
0.03
0.025
0.02
0.04
0.05
0.06
0.07
0.08
0.09
0.1
0.11
4.25 %
4.50 %
4.75 %
5.00 %
5.25 %
5.50 %
5.75 %

Thrust efficency for $\dot{m} = 70 \times 10^{-9} kg/s$

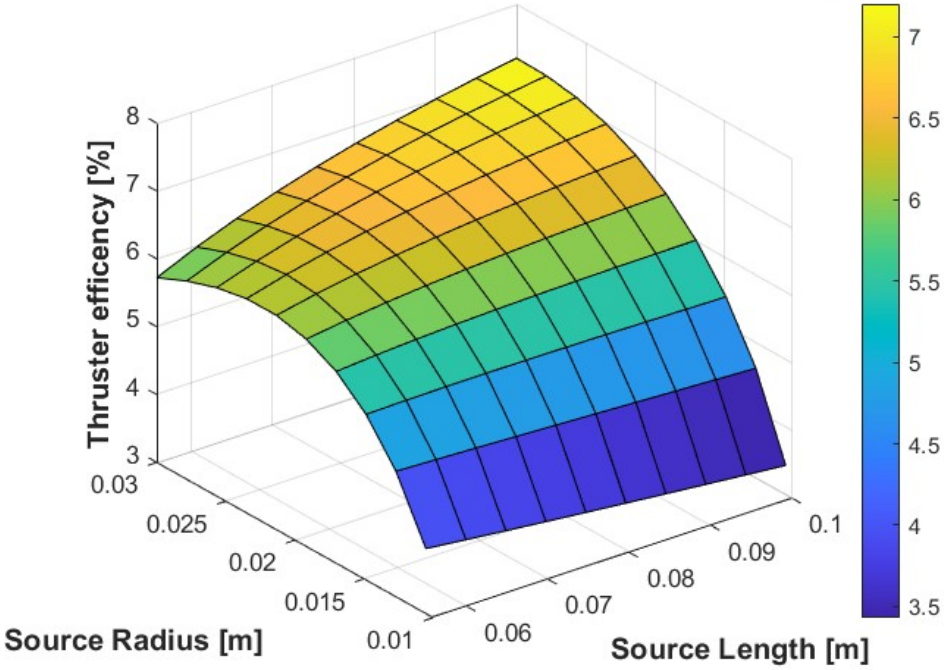

Thrust efficency for $\dot{m} = 90 \times 10^{-9} kg/s$

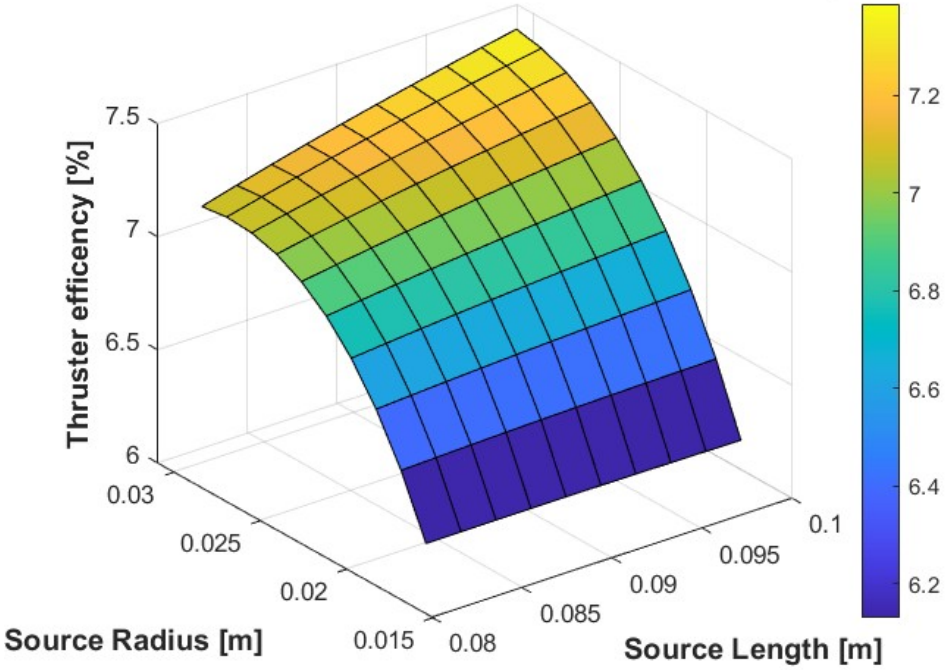

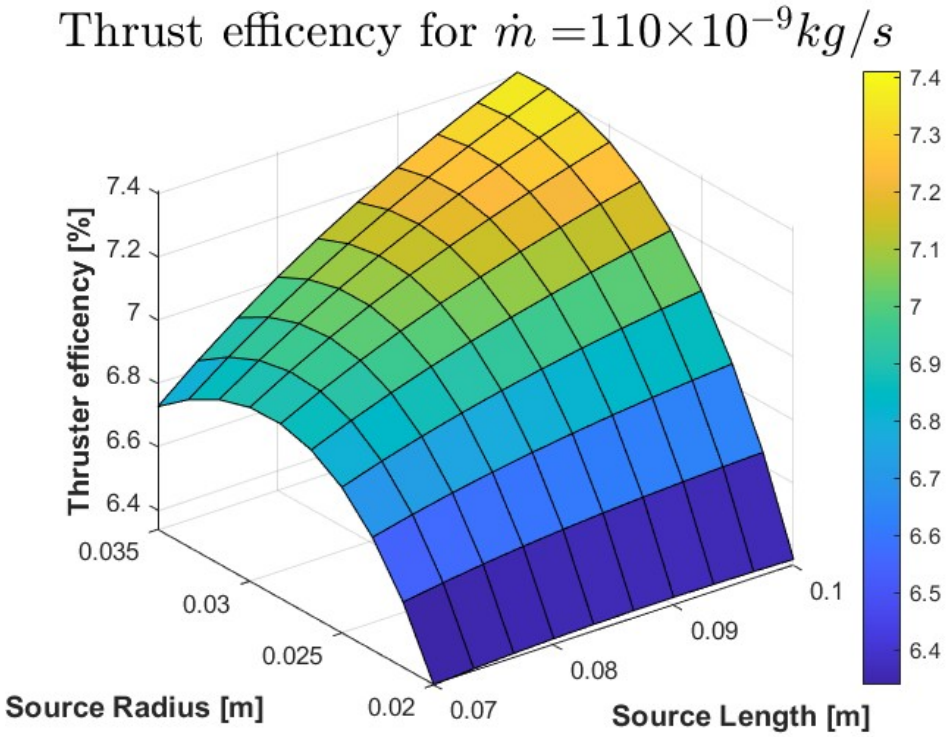
Thrust efficency for $\dot{m} = 110 \times 10^{-9} kg/s$
Thruster efficency [%]
7.4
7.2
7
6.8
6.6
6.4
Source Radius [m]
0.035
0.03
0.025
0.02
Source Length [m]
0.07
0.08
0.09
0.1
7.4
7.3
7.2
7.1
7
6.9
6.8
6.7
6.6
6.5
6.4

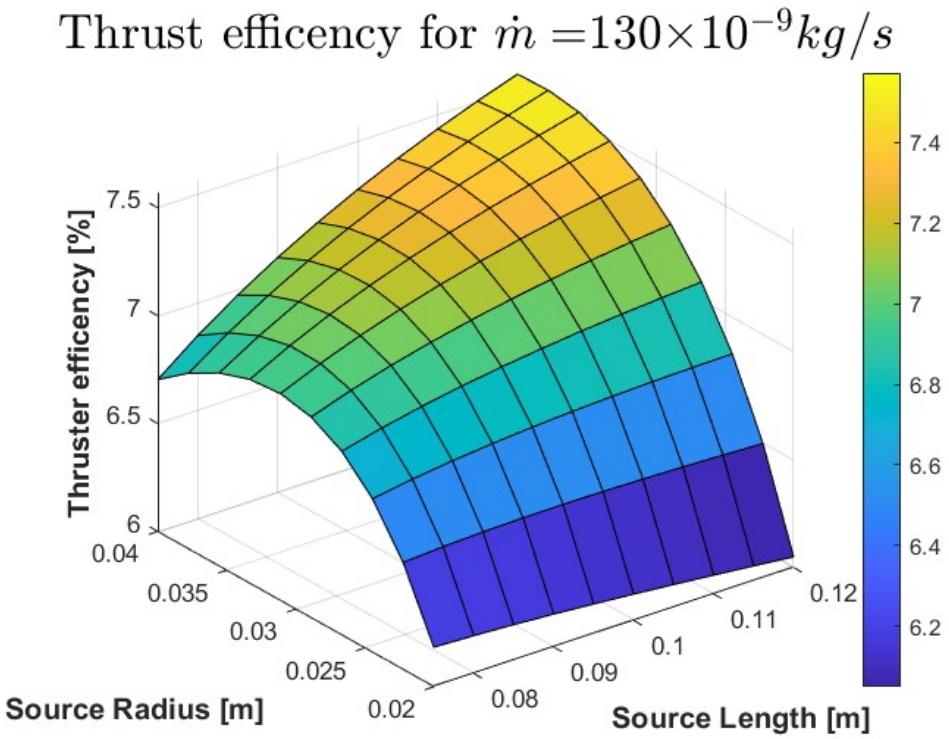
Thrust efficency for $\dot{m} = 130 \times 10^{-9} kg/s$
Thruster efficency [%]
7.5
7
6.5
6
Source Radius [m]
0.04
0.035
0.03
0.025
0.02
Source Length [m]
0.08
0.09
0.1
0.11
0.12
7.4
7.2
7
6.8
6.6
6.4
6.2

Thrust efficency for $\dot{m} = 150 \times 10^{-9} kg/s$

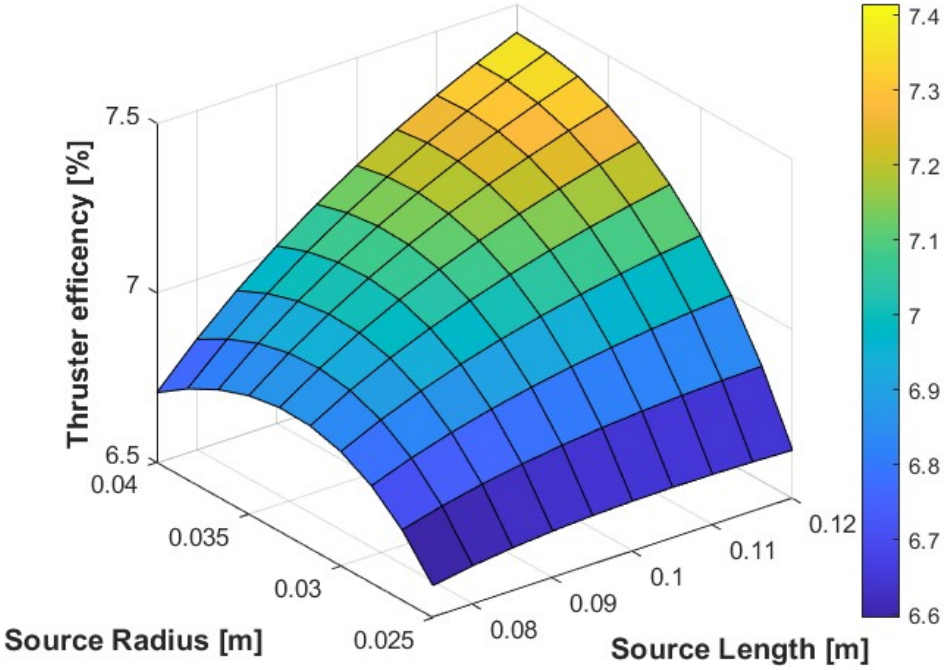

Thrust efficency for $\dot{m} = 170 \times 10^{-9} kg/s$

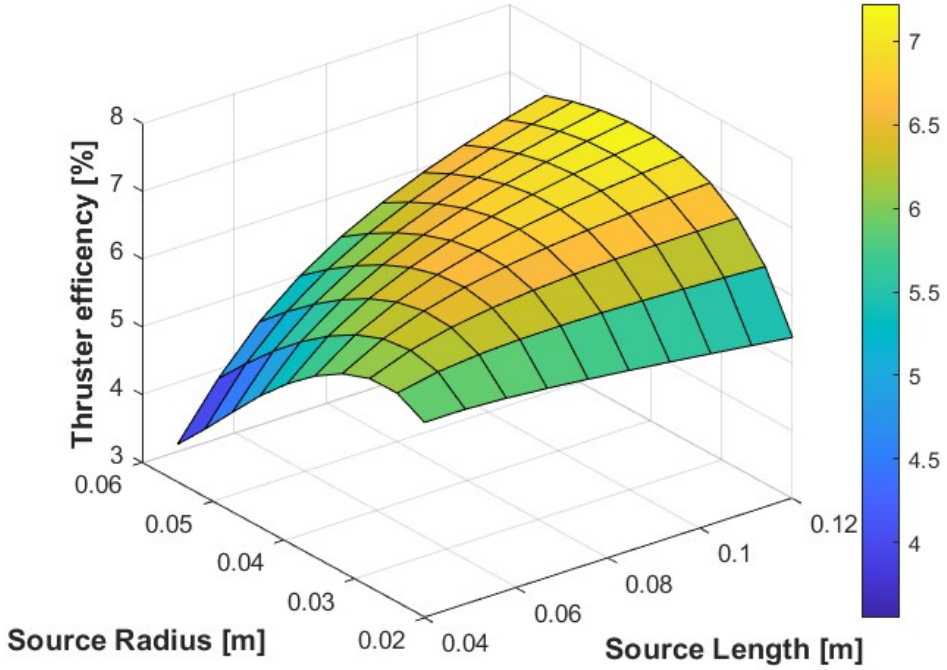

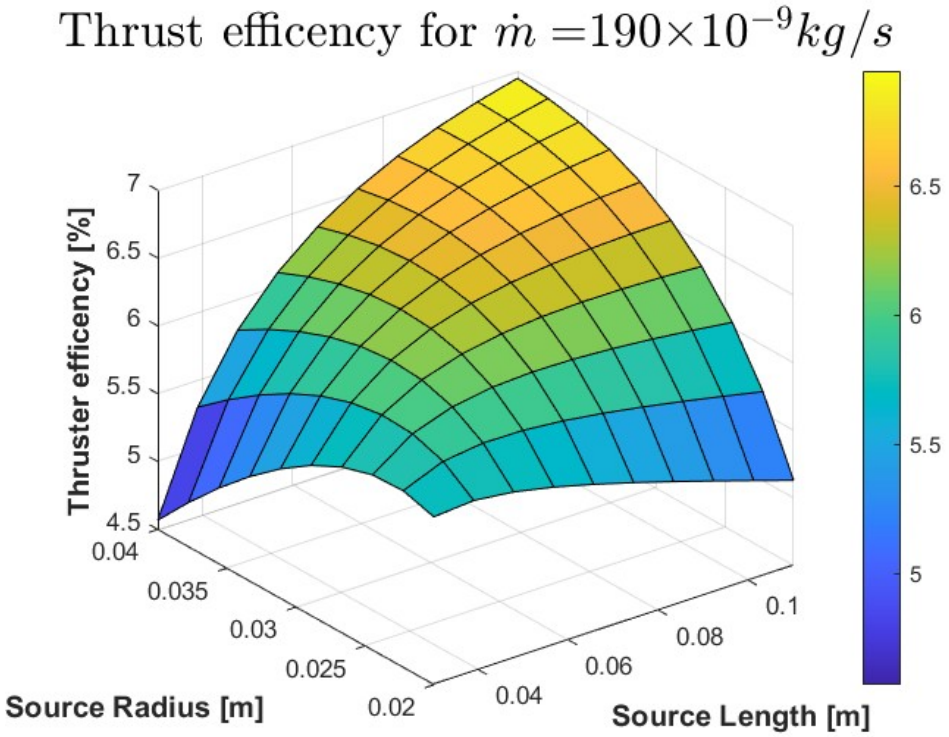
Thrust efficency for $\dot{m} = 190 \times 10^{-9} kg/s$
Thruster efficency [%]
7
6.5
6
5.5
5
4.5
0.04
0.035
0.03
0.025
0.02
Source Radius [m]
0.04
0.06
0.08
0.1
Source Length [m]
6.5
6
5.5
5

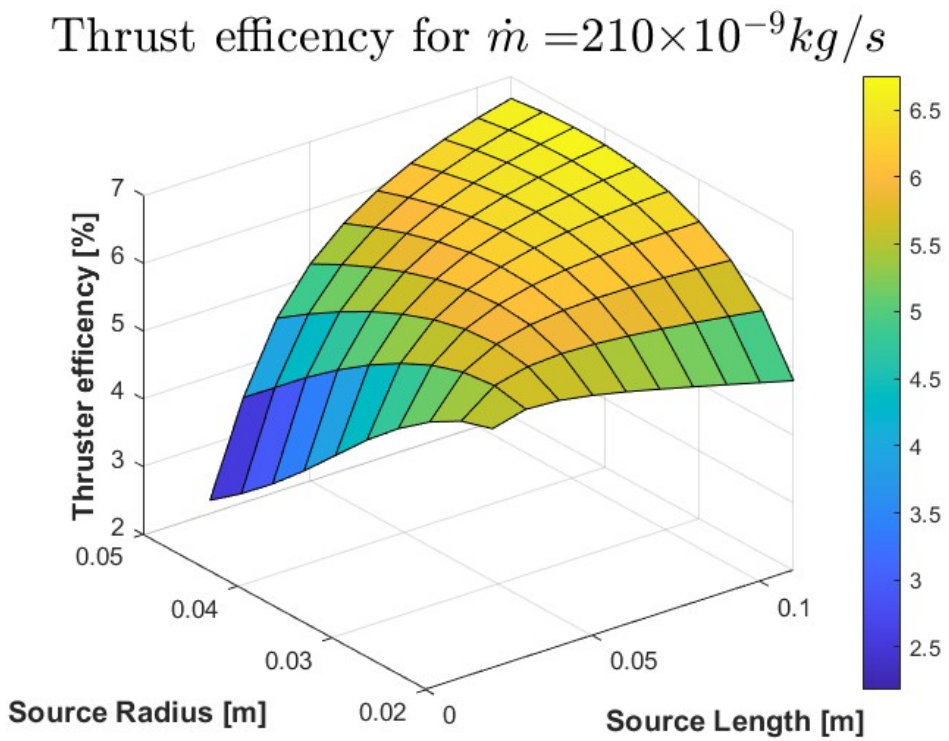
Thrust efficency for $\dot{m} = 210 \times 10^{-9} kg/s$
Thruster efficency [%]
7
6
5
4
3
2
0.05
0.04
0.03
0.02
Source Radius [m]
0
0.05
0.1
Source Length [m]
6.5
6
5.5
5
4.5
4
3.5
3
2.5

Thrust efficency for $\dot{m} = 250 \times 10^{-9} kg/s$

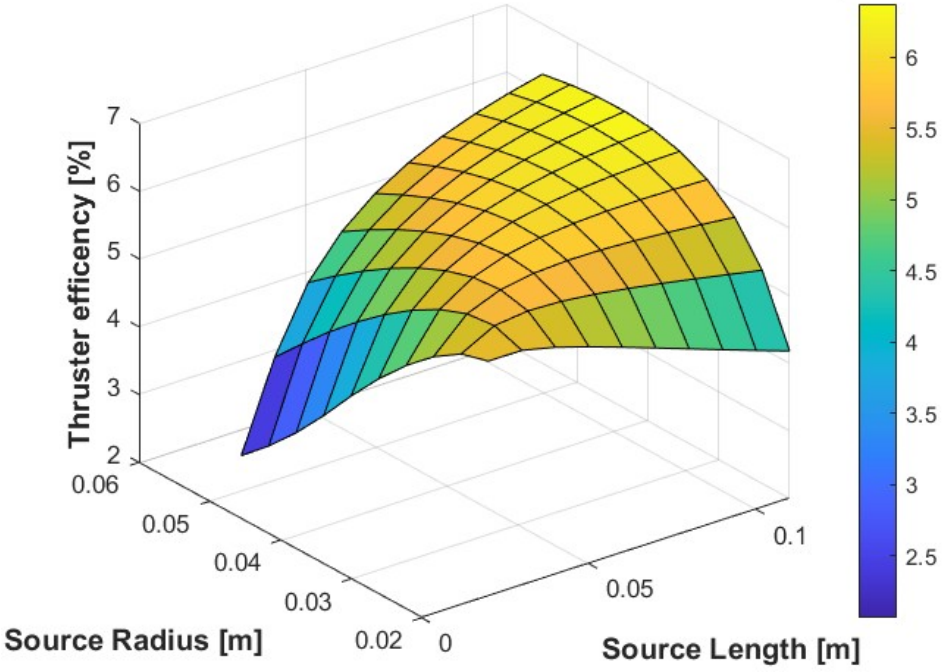

Thrust efficency for $\dot{m} = 270 \times 10^{-9} kg/s$

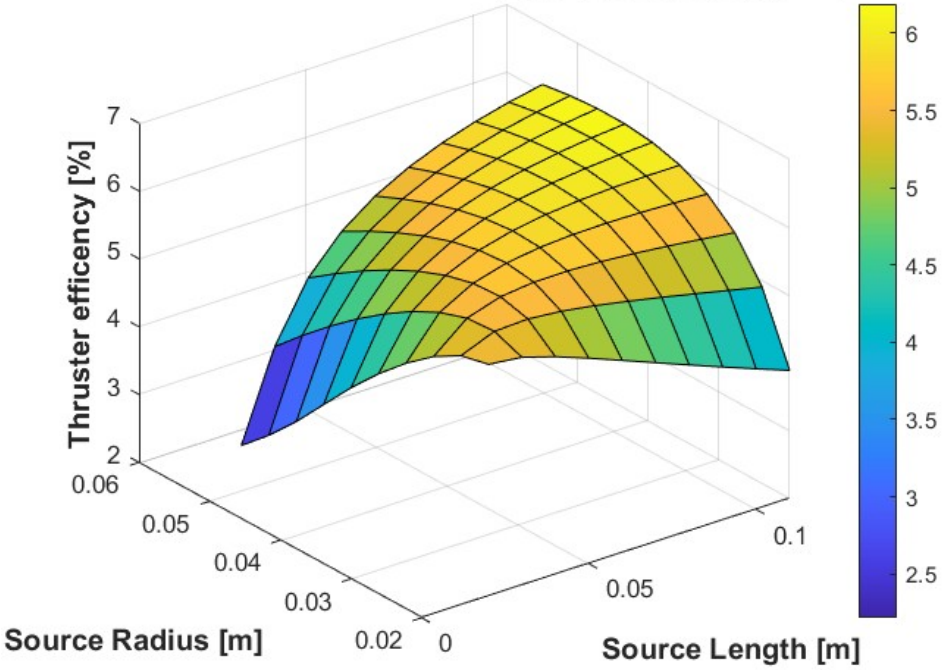

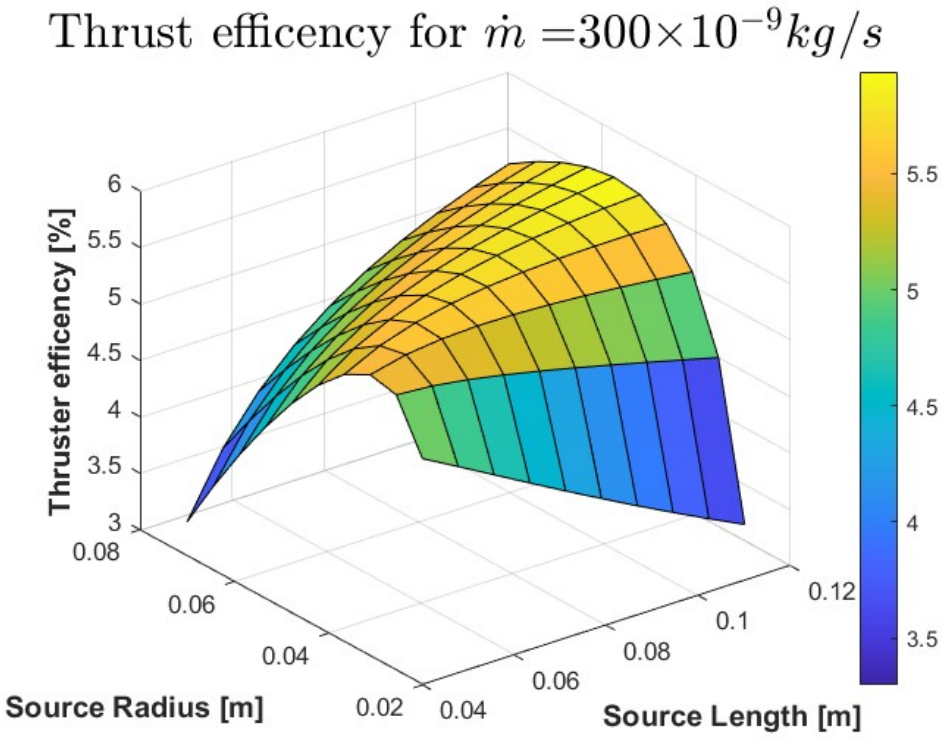
Thrust efficency for $\dot{m}$ =300×10^{-9}kg/s
Thruster efficency [%]
6
5.5
5
4.5
4
3.5
3
0.08
0.06
0.04
0.02
Source Radius [m]
0.04
0.06
0.08
0.1
0.12
Source Length [m]
5.5
5
4.5
4
3.5

Appendix B
Propulsive parameters plots in neighbourhood of optimized input values

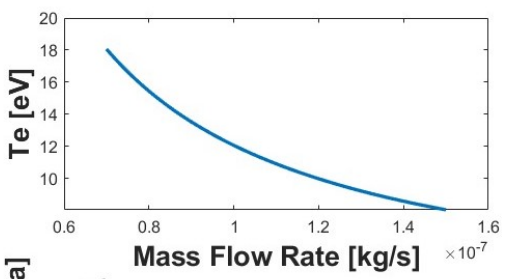
Te [eV]
20
18
16
14
12
10
0.6
0.8
1
1.2
1.4
1.6
Mass Flow Rate [kg/s]
×10-7

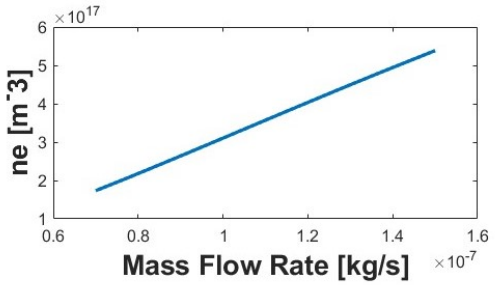
ne [m^3]
×10^17
6
5
4
3
2
1
0.6
0.8
1
1.2
1.4
1.6
Mass Flow Rate [kg/s]
×10-7

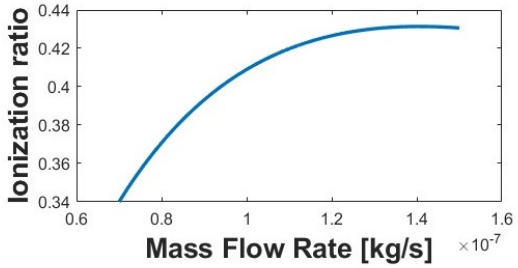
Ionization ratio
0.44
0.42
0.4
0.38
0.36
0.34
0.6
0.8
1
1.2
1.4
1.6
Mass Flow Rate [kg/s]
×10-7

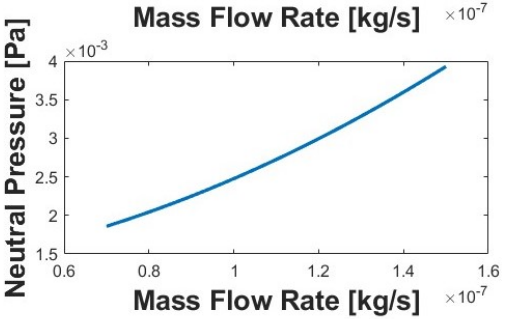
Neutral Pressure [Pa]
×10-3
4
3.5
3
2.5
2
1.5
0.6
0.8
1
1.2
1.4
1.6
Mass Flow Rate [kg/s]
×10-7

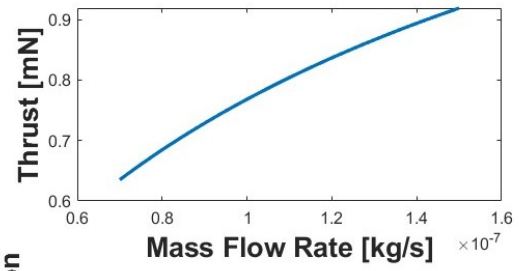
Thrust [mN]
0.9
0.8
0.7
0.6
0.6
0.8
1
1.2
1.4
1.6
Mass Flow Rate [kg/s]
×10-7

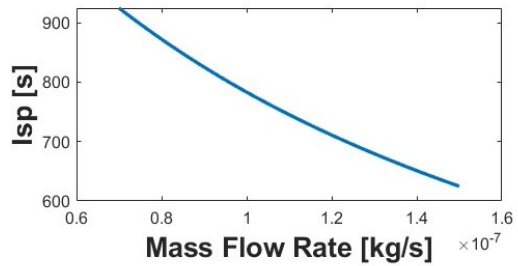
Isp [s]
900
800
700
600
0.6
0.8
1
1.2
1.4
1.6
Mass Flow Rate [kg/s]
×10-7

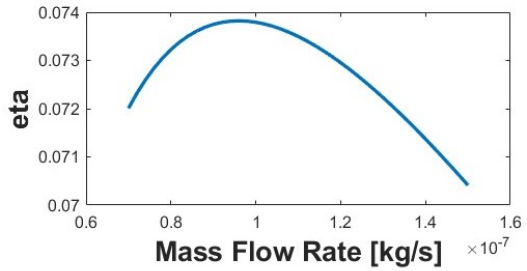
eta
0.074
0.073
0.072
0.071
0.07
0.6
0.8
1
1.2
1.4
1.6
Mass Flow Rate [kg/s]
×10-7

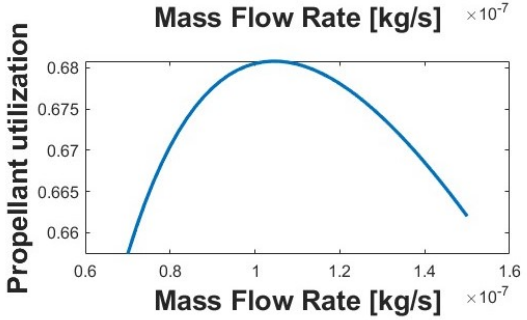
Propellant utilization
0.68
0.675
0.67
0.665
0.66
0.6
0.8
1
1.2
1.4
1.6
Mass Flow Rate [kg/s]
×10-7

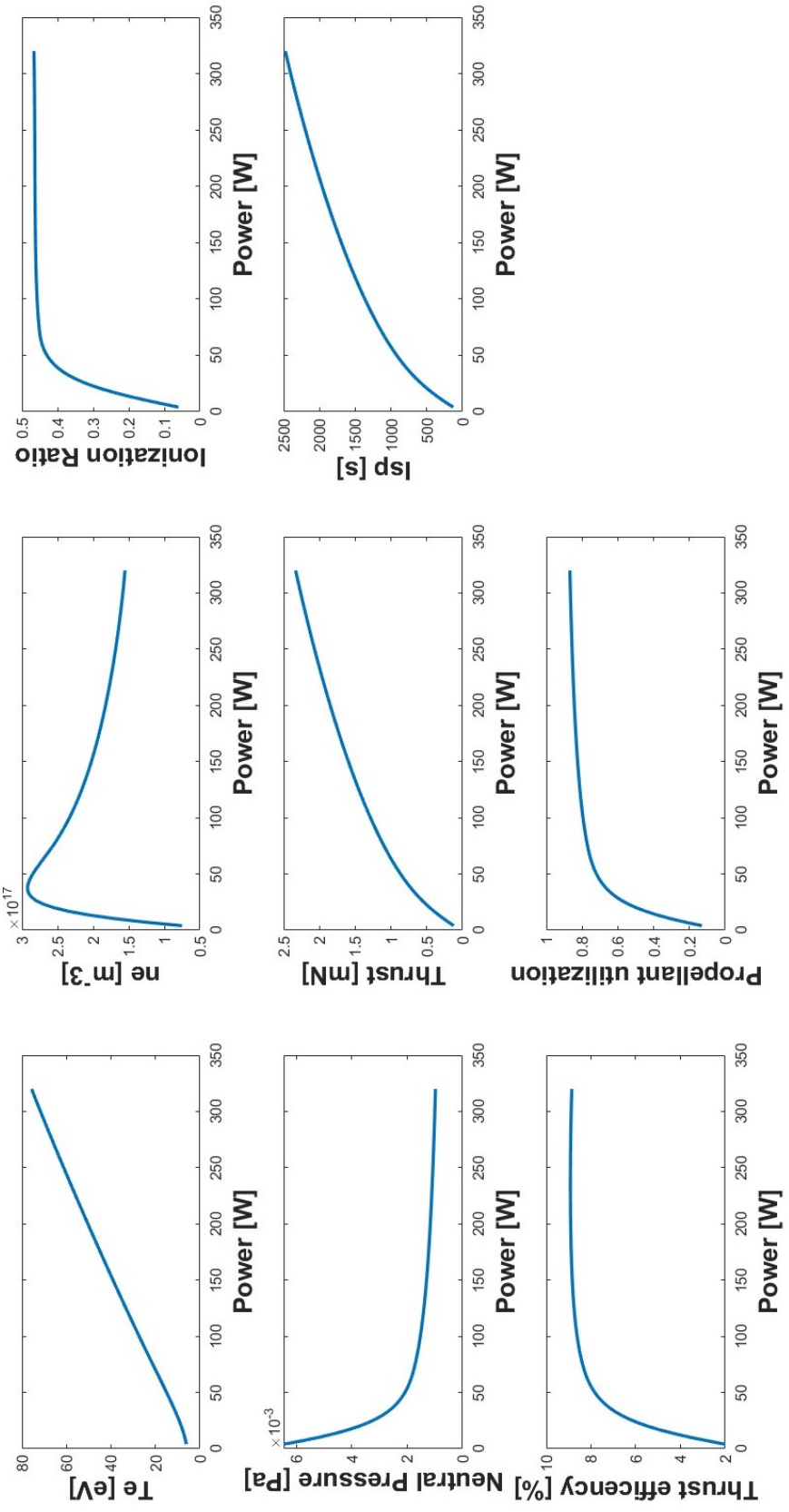
Te [eV]
Power [W]
Neutral Pressure [Pa]
Power [W]
Thrust efficency [%]
Power [W]
ne [m^3]
Power [W]
Thrust [mN]
Power [W]
Propellant utilization
Power [W]
Isp [s]
Power [W]
Ionization Ratio
Power [W]

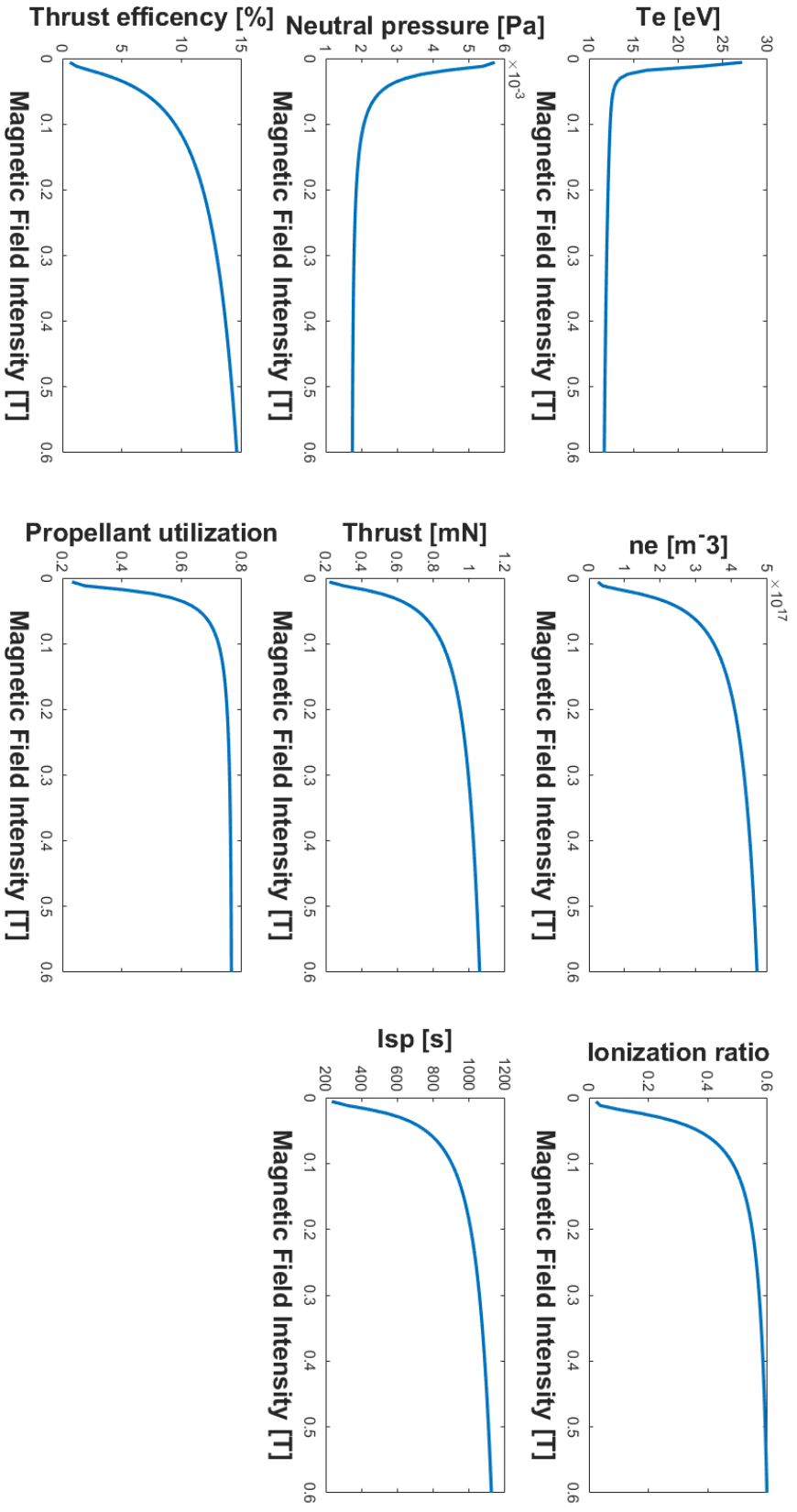
Te [eV]
Magnetic Field Intensity [T]
Neutral pressure [Pa]
×10^-3
Magnetic Field Intensity [T]
Thrust efficency [%]
Magnetic Field Intensity [T]
ne [m^-3]
×10^17
Magnetic Field Intensity [T]
Thrust [mN]
Magnetic Field Intensity [T]
Propellant utilization
Magnetic Field Intensity [T]
Ionization ratio
Magnetic Field Intensity [T]
Isp [s]
Magnetic Field Intensity [T]

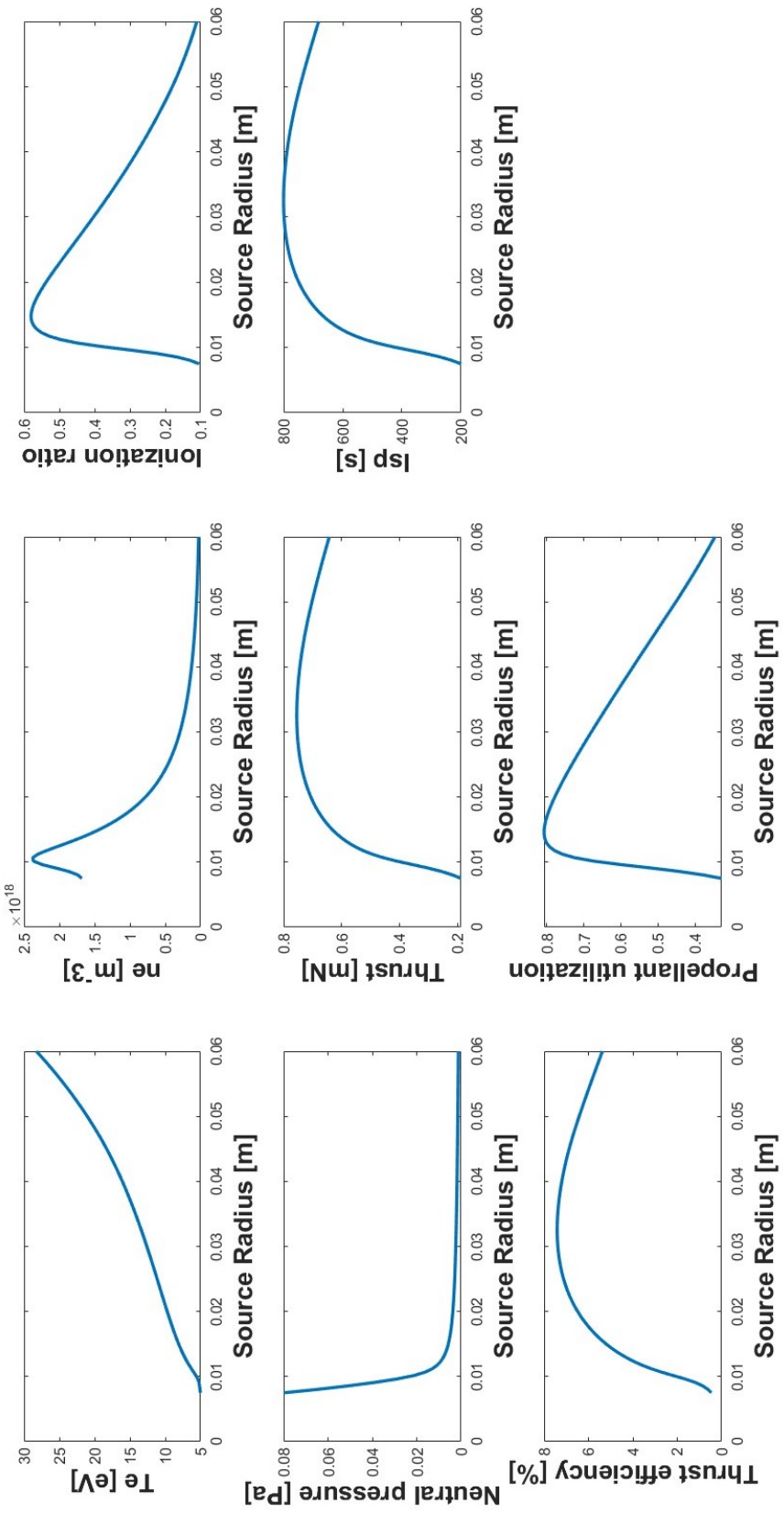
Ionization ratio
Isp [s]
ne [m^3]
Thrust [mN]
Propellant utilization
Te [eV]
Neutral pressure [Pa]
Thrust efficiency [%]
Source Radius [m]

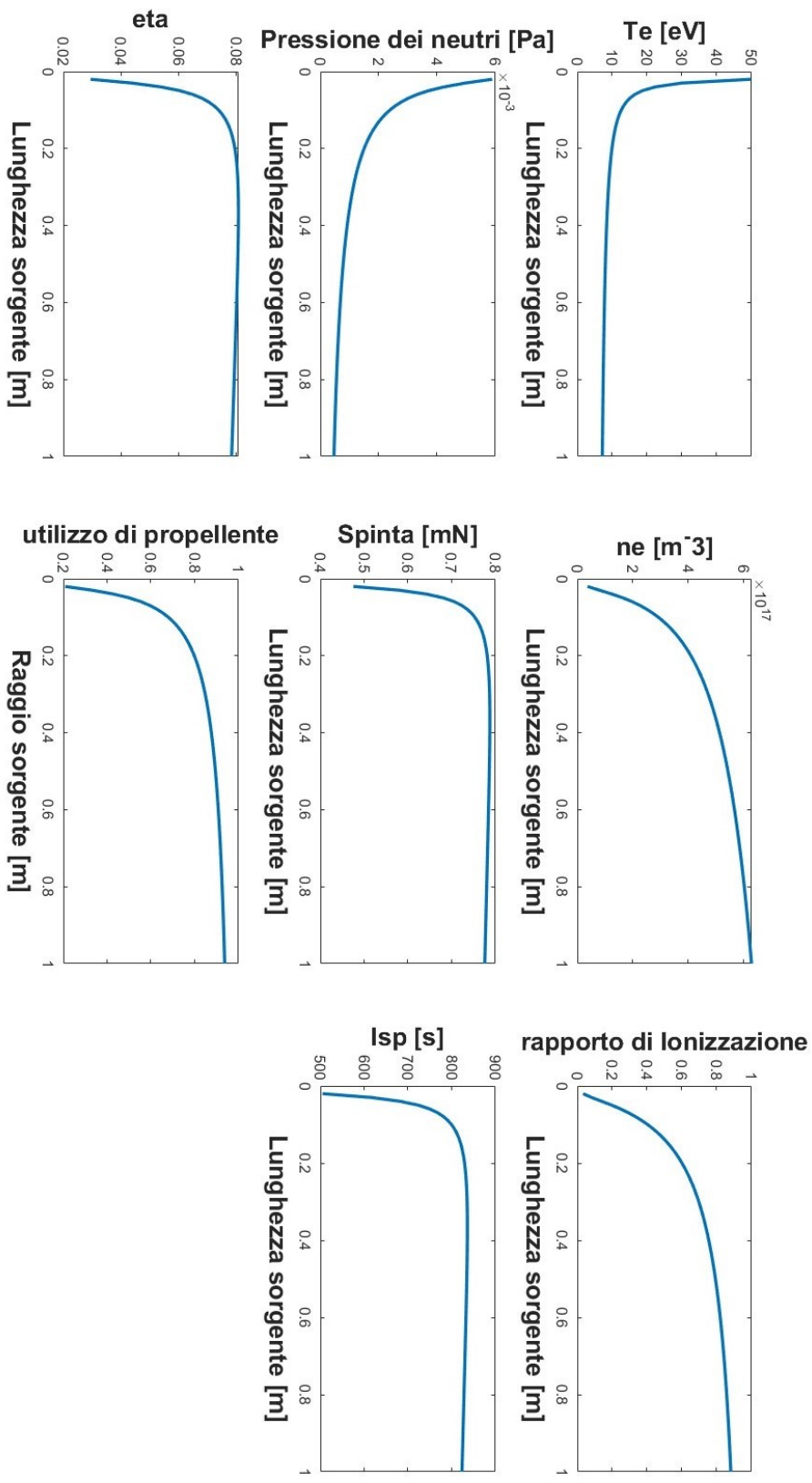
Te [eV]
Lunghezza sorgente [m]
Pressione dei neutri [Pa]
×10^-3
Lunghezza sorgente [m]
eta
Lunghezza sorgente [m]
ne [m^-3]
×10^17
Lunghezza sorgente [m]
Spinta [mN]
Lunghezza sorgente [m]
utilizzo di propellente
Raggio sorgente [m]
rapporto di Ionizzazione
Lunghezza sorgente [m]
Isp [s]
Lunghezza sorgente [m]

Bibliography

[1] Ane Aanesland, Stéphane Mazouffre, and Pascal Chabert. Space exploration technologies pegases-a new promising electric propulsion concept. *Europhysics News*, 42(6):28–31, 2011.

[2] Anna-Maria Theodora Andreescu, Maximilian-Vlad Teodorescu, Jeni Alina Popescu, Valeriu-Alexandru Vilag, and Adrian Stoicescu. Concept study of radio frequency (rf) plasma thruster for space propulsion. *INCAS Bulletin*, 8(4):15, 2016.

[3] Alexey V Arefiev and Boris N Breizman. Theoretical components of the vasimr plasma propulsion concept. *physics of plasmas*, 11(5):2942–2949, 2004.

[4] Nicolas Bellomo, Riccardo Di Roberto, Elena Toson, Daniele Pavarin, and Filippo Graziani. Regulus electric propulsion module iod in unisat-7 mission. 2019.

[5] Charles K Birdsall and A Bruce Langdon. *Plasma physics via computer simulation*. CRC press, 2018.

[6] FJ Bosi. *Development of global models of plasma systems for space propulsion*. PhD thesis, Ph. D. thesis, 2016.

[7] Rod W Boswell and Christine Charles. The helicon double layer thruster. In *28th International Electric Propulsion Conference, IEPC*, 2003.

[8] F Cannat, T Lafleur, J Jarrige, P Chabert, P-Q Elias, and D Packan. Optimization of a coaxial electron cyclotron resonance plasma thruster with an analytical model. *Physics of Plasmas*, 22(5):053503, 2015.

[9] Christine Charles. Plasmas for spacecraft propulsion. *Journal of Physics D: Applied Physics*, 42(16):163001, 2009.

[10] Filippo Cichocki, Adrián Domínguez-Vázquez, Mario Merino, and Eduardo Ahedo. Hybrid 3d model for the interaction of plasma thruster plumes with nearby objects. *Plasma Sources Science and Technology*, 26(12):125008, 2017.

[11] Dan M Goebel and Ira Katz. *Fundamentals of electric propulsion: ion and Hall thrusters*. John Wiley & Sons, 2008.

[12] Matteo Guaita, Mirko Magarotto, Marco Manente, Daniele Pavarin, and Michéle Lavagna. Semi-analytical model of a helicon plasma thruster. *IEEE Transactions on Plasma Science*, 50(2):425–438, 2022.

[13] Trevor Lafleur. Helicon plasma thruster discharge model. *Physics of Plasmas*, 21(4):043507, 2014.

[14] Michael A Lieberman and Allan J Lichtenberg. Principles of plasma discharges and materials processing. *MRS Bulletin*, 30(12):899–901, 1994.

[15] Mirko Magarotto, Marco Manente, Fabio Trezzolani, and Daniele Pavarin. Numerical model of a helicon plasma thruster. *IEEE Transactions on Plasma Science*, 48(4):835–844, 2020.

[16] Mirko Magarotto, Davide Melazzi, and Daniele Pavarin. 3d-virtus: Equilibrium condition solver of radio-frequency magnetized plasma discharges for space applications. *Computer Physics Communications*, 247:106953, 2020.

[17] M Manente, F Trezzolani, M Magarotto, E Fantino, A Selmo, N Bellomo, E Toson, and D Pavarin. Regulus: A propulsion platform to boost small satellite missions. *Acta Astronautica*, 157:241–249, 2019.

[18] Manuel Martinez-Sanchez, Jaume Navarro-Cavallé, and Eduardo Ahedo. Electron cooling and finite potential drop in a magnetized plasma expansion. *Physics of Plasmas*, 22(5):053501, 2015.

[19] Dmytro Rafalskyi and Ane Aanesland. Coincident ion acceleration and electron extraction for space propulsion using the self-bias formed on a set of rf biased grids bounding a plasma source. *Journal of Physics D: Applied Physics*, 47(49):495203, 2014.

[20] Adam Shabshelowitz, Alec D Gallimore, and Peter Y Peterson. Performance of a helicon hall thruster operating with xenon, argon, and nitrogen. *Journal of Propulsion and Power*, 30(3):664–671, 2014.

[21] George P Sutton and Oscar Biblarz. *Rocket propulsion elements*. John Wiley & Sons, 2016.